Synthesis and Stereochemical Analysis of the $[Fe_4(NO)_4(\mu_3\text{-}S)_4]^n$ Series (n = 0, -1) Which Possesses a Cubanelike Fe_4S_4 Core: Direct Evidence for the Antibonding Tetrametal Character of the Unpaired Electron upon a One-Electron Reduction of a Completely Bonding Tetrahedral Metal Cluster

Cynthia Ting-Wah Chu, Frederick Yip-Kwai Lo, and Lawrence F. Dahl*

Contribution from the Department of Chemistry, University of Wisconsin—Madison, Madison, Wisconsin 53706. *Received September 28, 1981*

Abstract: Presented herein are the preparations, properties, and structural determinations of the $[Fe_4(NO)_4(\mu_3\text{-}S)_4]^-$ monoanion and its neutral parent, which have provided a means of examination of the geometrical changes associated with the 0/-1 electron-transfer couple for a cubanelike Fe_4S_4 core coordinated to π-acidic nitrosyl ligands. The sought-after black $Fe_4(NO)_4(\mu_3\text{-}S)_4$ tetramer was synthesized in 20% yield by the reaction of $Hg[Fe(CO)_3NO]_2$ with sulfur under toluene reflux. Cyclic voltammetric measurements of $Fe_4(NO)_4(\mu_3\text{-}S)_4$ in CH_2Cl_2 solution revealed two reversible 0/-1 and -1/-2 couples. Its reduction by potassium benzophenone in toluene solution containing 2,2,2-cryptand afforded the corresponding black monoanion (as the $[K(2,2,2\text{-crypt})]^+$ salt), which from room-temperature susceptibility measurements is presumed to contain one unpaired electron. Both compounds are reasonably air stable in crystalline form but decompose readily in solution. The most striking structural feature found upon the reduction of the 60-electron $Fe_4(NO)_4(\mu_3\text{-}S)_4$ cluster to its 61-electron monoanion is that the idealized cubic T_d-$\bar{4}3m$ Fe_4S_4 core containing a completely bonding iron tetrahedron of average length 2.651 Å in the neutral parent is slightly but significantly deformed in the monoanion toward tetragonal D_{2d}-$\bar{4}2m$ symmetry, as evidenced by (1) a lengthening of the two Fe–Fe bonds normal to the resulting one S_4-$\bar{4}$ axis by 0.053 Å (to 2.703 (1) and 2.704 (1) Å) relative to the average lengthening of the other four Fe–Fe bonds by 0.037 Å (to a mean 2.688 Å and range 2.682 (1)–2.695 (1) Å) and (2) the six nonbonding S···S distances, which are equivalent under T_d symmetry, dividing into an inverse pattern of two shorter distances (of 3.493 (2) and 3.499 (2) Å) and four longer distances (of range 3.511 (2)–3.520 (2) Å and mean 3.517 Å). A concomitant average increase of only 0.014 Å in the 12 Fe–S bond lengths of the Fe_4S_4 core is observed upon reduction to the monoanion, for which the partitioned 8 and 4 equivalent Fe–S distances under D_{2d} symmetry possess identical mean lengths of 2.231 Å. These architectural variations can be rationalized via a qualitative metal cluster model that predicts that the unpaired electron in the monoanion occupies (under T_d symmetry) a triply degenerate t_1 level of largely tetrairon-antibonding character, which thereby produces the observed tetragonal distortion via a first-order Jahn–Teller vibronic effect; the relatively large bond-length increases in all six (instead of just two) Fe–Fe bonds suggest that the HOMO in the monoanion has considerable antibonding character among all six pairs of iron atoms. These collective findings provide a basic understanding of the geometrical differences imposed by one-electron redox couples on the Fe_4S_4 cores of the structurally determined $[Fe_4(NO)_4(\mu_3\text{-}S)_4]^n$ series (n = 0, 1-), the $[Fe_4(\eta^5\text{-}C_5H_5)_4(\mu_3\text{-}S)_4]^n$ series (n = 0, 1+, 2+), and the $[Fe_4(SPh)_4(\mu_3\text{-}S)_4]^n$ series (n = 2-, 3-), whose members are synthetic analogues of the four-iron active sites of ferredoxin proteins. A comparative structural bonding analysis shows that the markedly different redox-generated changes in the geometries of the Fe_4S_4 cores of these three series containing dissimilar terminal ligands may be correlated with their different electronic configurations. Crystals of $Fe_4(NO)_4(\mu_3\text{-}S)_4$ are monoclinic with symmetry $P2_1/n$ and lattice constants a = 12.350 (3) Å, b = 9.627 (7) Å, c = 10.407 (4) Å, and β = 106.66 (3)°; d_{calcd} = 2.59 g/cm^3 for Z = 4 and V = 1202.3 (8) Å^3. Anisotropic least-squares refinement of 1384 independent diffractometry data with $I \geq 2\sigma(I)$ converged at $R_1(F)$ = 3.2% and $R_2(F)$ = 4.2%. Crystals of $[K(2,2,2\text{-crypt})]^+[Fe_4(NO)_4(\mu_3\text{-}S)_4]^-$ are triclinic, space group $P\bar{1}$, with a = 12.766 (4) Å b = 13.118 (4) Å, c = 10.172 (3) Å, α = 95.96 (2)°, β = 93.70 (2)°, γ = 85.68 (2)°, V = 1686.6 (8) Å^3, and d_{calcd} = 1.75 g/cm^3 for Z = 2. Anisotropic least-squares refinement gave $R_1(F)$ = 4.6% and $R_2(F)$ = 5.8% for 4526 independent diffractometry data with $I \geq 2\sigma(I)$.

Introduction

The research reported herein is a consequence of our preparative and stereochemical analyses of $[M_4L_4(\mu_3\text{-}X)_4]^n$ clusters containing cubanelike M_4X_4 cores in order to establish a systematic correlation between geometry and electronic configuration. This work has resulted in the syntheses and physicochemical characterizations of a number of cyclopentadienyl metal chalcogenide and pnictide tetramers which presently include the $[Fe_4(\eta^5\text{-}C_5H_5)_4(\mu_3\text{-}X)_4]^n$ series (for X = S, n = 0,[1] 1+,[2] 2+;[3] for X = Se, n = 0,[4] 1+,[5] 2+;[4] for X = Te, n = 2+[5]), the $[Co_4(\eta^5\text{-}C_5H_5)_4(\mu_3\text{-}X)_4]^n$ series (for X = P, n = 0;[6] for X = As, n = 0[7]), the $Co_4(\eta^5\text{-}C_5H_5)_4(\mu_3\text{-}X)_4]^n$ series (for X = S, n = 0,[8] 1+;[8] for X = Te, n = 0, 2+[5]), and the neutral $Mo_4(\eta^5\text{-}C_5H_5)_4(\mu_3\text{-}S)_4$.[9]

Our activity in exploring the structural-bonding influences produced by the formal substitution of a terminal π-acidic nitrosyl ligand in place of the tridentate cyclopentadienyl ligand initially led to the preparation of $Co_4(NO)_4(\mu_3\text{-}NCMe_3)_4$[10] and $Fe_4(NO)_4(\mu_3\text{-}S)_2(\mu_3\text{-}NCMe_3)_2$.[11,12] The latter molecule, which possesses a cubanelike $Fe_2S_2N_2$ core of idealized C_{2v} geometry with a completely bonding iron tetrahedron, provided the incentive that resulted in the successful synthesis and characterization of

(1) (a) Wei, C. H.; Wilkes, G. R.; Treichel, P. M.; Dahl, L. F. *Inorg. Chem.* **1966**, *5*, 900–905. (b) Schunn, R. A.; Fritchie, C. J., Jr.; Prewitt, C. T. *Ibid.* **1966**, *5*, 892–899.
(2) Trinh-Toan; Fehlhammer, W. P.; Dahl, L. F. *J. Am. Chem. Soc.* **1977**, *99*, 402–407.
(3) Trinh-Toan; Teo, B. K.; Ferguson, J. A.; Meyer, T. J.; Dahl, L. F. *J. Am. Chem. Soc.* **1977**, *99*, 408–416.
(4) Roder, R. M. Ph.D. Thesis, University of Wisconsin—Madison, Madison, WI, 1973.
(5) Szmanda, C. R. Ph.D. Thesis, University of Wisconsin—Madison, Madison, WI, 1979.
(6) Simon, G. L.; Dahl, L. F. *J. Am. Chem. Soc.* **1973**, *95*, 2175–2183.
(7) Paquette, M. S. Ph.D. Thesis, University of Wisconsin—Madison, Madison, WI, 1978.
(8) Simon, G. L.; Dahl, L. F. *J. Am. Chem. Soc.* **1973**, *95*, 2164–2174.
(9) Burger, T. J.; Wei, C. H.; Vergamini, P. J.; Dahl, L. F., to be submitted for publication.
(10) Gall, R. S.; Connelly, N. G.; Dahl, L. F. *J. Am. Chem. Soc.* **1974**, *96*, 4017–4019.
(11) Gall, R. S.; Chu, C. T.-W.; Dahl, L. F. *J. Am. Chem. Soc.* **1974**, *96*, 4019–4023.
(12) Chu, C. T.-W.; Gall, R. S.; Dahl, L. F. *J. Am. Chem. Soc.* **1982**, *104*, 737–746.

0002-7863/82/1504-3409$01.25/0 © 1982 American Chemical Society

the corresponding electronically equivalent $Fe_4(NO)_4(\mu_3\text{-}S)_4$. Of prime interest were the particular geometrical dissimilarities found among its Fe–Fe-bonded cubic T_d Fe_4S_4 core and the Fe_4S_4 cores of the $[Fe_4(\eta^5\text{-}C_5H_5)_4(\mu_3\text{-}S)_4]^n$ series (n = 0,[1] 1+,[2] 2+[3]) and the $[Fe_4(SCH_2Ph)_4(\mu_3\text{-}S)_4]^{2-}$ dianion,[13] which was the earliest crystallographically determined member of the $[Fe_4(SR)_4(\mu_3\text{-}S)_4]^n$ series (n = 1–, 2–, 3–) shown from extensive structural and physicochemical studies by Holm, Ibers, and co-workers[14] to be the first synthetic analogues of the Fe_4S_4 cluster units in bacterial ferredoxins and in the high-potential iron proteins. The application[11] of the qualitative MO cluster model.[3,15] showed that the marked stereochemical differences observed among these three types of Fe_4S_4 clusters could be readily attributed to their possessing entirely different electronic configurations involving each of the three kinds of possible energetic distribution patterns composed of the tetrairon symmetry combinations of the valence d AO's. Furthermore, this metal cluster model suggested that a one-electron reduction of cubic T_d-$\bar{4}3m$ $Fe_4(NO)_4(\mu_3\text{-}S)_4$ to its monoanion would involve the unpaired electron occupying a triply degenerate molecular orbital of large antibonding tetrairon character which, via a first-order Jahn–Teller mechanism, would be expected to produce a vibronically allowed tetragonal D_{2d}-$\bar{4}2m$ geometry with a relative lengthening either of two or conversely of the other four Fe–Fe distances in the completely bonding iron tetrahedron of the neutral parent.

The observation that cyclic voltammetric measurements of $Fe_4(NO)_4(\mu_3\text{-}S)_4$ exhibited two reversible, one-electron reduction waves, indicating the existence of both the monoanion (n = 1–) and dianion (n = 2–),[16] stimulated intensive efforts to isolate and structurally characterize the monoanion as an operational test of our bonding hypothesis. Initial attemps were frustratingly unsuccessful. Although the reductant cobaltocene yielded $[Co(\eta^5\text{-}C_5H_5)_2]^+[Fe_4(NO)_4(\mu_3\text{-}S)_4]^-$, an X-ray diffraction investigation of the isolated crystals failed to resolve the detailed crystal structure on account of a complicated crystal disorder and/or crystal twinning. Reductions carried out with Na/Hg amalgam in THF at room temperature also produced the monoanion, but all attempts to isolate suitable untwinned crystals of the monoanion by exchange of the Na^+ ion in solution with either tetraphenylarsonium or bis(triphenylphosphine)iminium cations were in vain. These endeavors included (1) the unexpected isolation and detailed crystallographic analysis[17] of the tetraphenylarsonium salt of the classical Roussin black $[Fe_4(NO)_7(\mu_3\text{-}S)_3]^-$ monoanion, whose overall architecture had been previously ascertained from an early X-ray photographic study by Johansson and Lipscomb[18] of its monohydrated cesium salt, and (2) the isolation of crystals of $[AsPh_4]^+[Fe_4(NO)_4(\mu_3\text{-}S)_4]^-$, which however, from an X-ray diffraction examination did not yield the detailed configuration of the monoanion presumably due to a crystal twinning and/or crystal disorder. Other methods in recrystallization of the $[Fe_4(NO)_4(\mu_3\text{-}S)_4]^-$ monoanion were hindered by the tendency for the monoanion to decompose to FeS and/or the Roussin black monoanion. The inherent instability of the $[Fe_4(NO)_4(\mu_3\text{-}S)_4]^-$ monoanion is further evidenced by the disproportionation of the $Fe_4(NO)_4(\mu_3\text{-}S)_4$ molecule in THF solution to Fe^{2+} and the Roussin black anion when a solution of the neutral $Fe_4(NO)_4(\mu_3\text{-}S)_4$ molecule is exposed to air. On the other hand, our simultaneous efforts to prepare and isolate the $[Fe_4(NO)_4(\mu_3\text{-}S)_2(\mu_3\text{-}NCMe_3)_2]^-$ monoanion in crystalline form as the bis(triphenylphosphine)iminium salt in order to perform an X-ray diffraction study were successful, and a resulting comparative analysis[12] of the structural features of this $[Fe_4(NO)_4(\mu_3\text{-}S)_2(\mu_3\text{-}NCMe_3)_2]^n$ series (n = 0, –1) suggested that the monoanion of the $Fe_4(NO)_4(\mu_3\text{-}S)_4$ molecule should indeed possess a tetragonal D_{2d} configuration with two relatively longer Fe–Fe bonds perpendicular to the S_4-$\bar{4}$ axis.

Herein are reported the results of our ultimate preparation of the $[Fe_4(NO)_4(\mu_3\text{-}S)_4]^-$ monoanion by reduction of the neutral parent with potassium benzophenone in the presence of an appropriate molar quantity of 2,2,2-cryptand (a macrocyclic inclusion ligand) in order to stabilize the monoanion as the $[K(2,2,2\text{-crypt})]^+$ salt. The isolated crystals were chracterized by IR spectroscopy, Mössbauer spectroscopy, and a magnetic susceptibility measurement as well as by an X-ray diffraction study. A comparative structural analysis of this $[Fe_4(NO)_4(\mu_3\text{-}S)_4]^n$ series (n = 0, 1–) not only has provided an operational test of our hypothesized structure based upon the corresponding $[Fe_4(NO)_4(\mu_3\text{-}S)_2(\mu_3\text{-}NCMe_3)_2]^n$ series (n = 0, 1–) but also has furnished experimentally convincing evidence in support of our qualitative metal cluster model that establishes a self-consistent set of structural-bonding interrelationships for cubanelike M_4X_4 cores with different terminal ligands. Also presented are the details of the preparation and physicochemical characterization of $Fe_4(NO)_4(\mu_3\text{-}S)_4$, for which a preliminary account has been previously given.[11]

Experimental Section

Preparations and Properties. General Comments. All reactions and manipulations were carried out under nitrogen in Schlenk-type apparatus. Solution transfers were carried out with stainless-steel tubes. $Hg[Fe(CO)_3(NO)]_2$ was prepared from $Fe(CO)_5$, KNO_2, and $Hg(CN)_2$ by the method of King.[19] The 2,2,2-cryptand ligand was obtained from PCR Research Chemicals, Inc., $Hg(CN)_2$ from Apache Chemicals, Inc., and $Fe(CO)_5$ from Alfa. These chemicals were used without further purification. Solvents were dried and distilled before use. The experiments described below are typical in that a given experiment was carried out more than once, sometimes under slightly different reaction conditions.

$Fe_4(NO)_4(\mu_3\text{-}S)_4$. This compound was prepared by the reaction of 1.01 g (1.8 mmol) of $Hg[Fe(CO)_3NO]_2$ and 0.18 g (5.4 mmol) of sulfur under reflux with vigorous stirring in 30 mL of toluene for 16 h. The color of the solution turned from reddish brown to black. After being cooled, the resultant mixture was extracted with toluene. The unextracted substances consist mainly of mercuric sulfide, elemental mercury, and $HgFe(CO)_4$, which is formed upon a heating of $Hg[Fe(CO)_3NO]_2$. Removal of the toluene under vacuum from the black solution gave ca. 80 mg (20% yield) of the black solid identified as $Fe_4(NO)_4(\mu_3\text{-}S)_4$. Attempts to run the same reaction at lower temperatures in hexane or benzene were unsuccessful. Analogous reactions performed with cyclohexene sulfide, propylene sulfide, or $(Me_3CN)_2S$ together with H_2S as the sulfur reagent also failed to give the desired product.

$Fe_4(NO)_4(M_3\text{-}S)_4$ is moderately insoluble in hexane but soluble in toluene, CH_2Cl_2, and THF. Crystals were grown for X-ray analysis by slow evaporation of a chloroform–octane solution under nitrogen. Its infrared spectra (taken on a Digilab FTS-20 Fourier transform spectrometer with 2.0-cm^{-1} resolution) exhibited one sharp nitrosyl stretching frequency at 1760 cm^{-1} in the solid state (KBr pellet) and at 1790 cm^{-1} in CH_2Cl_2 solution. The diamagnetism of $Fe_4(NO)_4(\mu_3\text{-}S)_4$ was indicated by the NMR method, which showed no shift of the ^1H resonance of an internal standard, *tert*-butyl alcohol (ca. 2%), in $CDCl_3$.

Cyclic voltammetric measurements (performed with a Princeton Applied Research Electrochemistry System, Model 170) of $Fe_4(NO)_4(\mu_3\text{-}S)_4$ were obtained at a platinum-bead electrode in a 0.1 M CH_2Cl_2 solution containing freshly crystallized tetra-*n*-butylammonium hexafluorophosphate (TBAH). All electrochemical measurements were made vs. a standard saturated calomel electrode.

$[Co(\eta^5\text{-}C_5H_5)_2]^+[Fe_4(NO)_4(\mu_3\text{-}S)_4]^-$. This salt of the monoanion was prepared by reduction with cobaltocene. An equal molar ratio of cobaltocene in toluene was added to $Fe_4(NO)_4(\mu_3\text{-}S)_4$ in chloroform. After 2 h of stirring under N_2 atmosphere, the mixture was filtered and washed with chloroform. The precipitate was then extracted with acetonitrile,

(13) Averill, B. A.; Herskovitz, T.; Holm, R. H.; Ibers, J. A. *J. Am. Chem. Soc.* **1973**, *95*, 3523–3534.

(14) Ibers, J. A.; Holm, R. H. *Science* (*Washington, D.C.*) **1980**, *209*, 223–35 and references cited therein.

(15) (a) Teo, B. K. Ph.D. Thesis, University of Wisconsin—Madison, Madison, WI, 1973. (b) Dahl, L. F. Abstracts of Papers, 165th National Meeting of the American Chemical Society, Dallas, TX, April 1973, American Chemical Society: Washington, D.D.; INOR 6. (c) Teo, B. K.; Dahl, L. F., to be submitted for publication.

(16) The initial cyclic voltammetric measurements resulted in a misassignment of the two one-electron, reversible waves in terms of the neutral $Fe_4(NO)_4(\mu_3\text{-}S)_4$ molecule undergoing both a one-electron oxidation and a one-electron reduction. Subsequent electrochemical measurements, which included an examination of the integrated current as a function of voltage for the bulk solution of the neutral parent, unambiguously established that the observed $E_{1/2}$ values instead correspond to the $[Fe_4]^0/[Fe_4]^-$ and $[Fe_4]^-/[Fe_4]^{2-}$ couples, where $[Fe_4]$ denotes $Fe_4(NO)_4(\mu_3\text{-}S)_4$.

(17) Chu, C. T.-W.; Dahl, L. F. *Inorg. Chem.* **1977**, *16*, 3245–3251.

(18) Johansson, G.; Lipscomb, W. N. *Acta Crystallogr.* **1958**, *11*, 594–598 and references cited therein.

(19) King, R. B. "Organometallic Synthesis"; Academic Press: New York, 1965; Vol. I, pp 165–166.

from which a vacuum-dried sample was obtained. Black platelike crystals of $[Co(\eta^5\text{-}C_5H_5)_2]^+[Fe_4(NO)_4(\mu_3\text{-}S)_4]^-$ were isolated by a slow vapor-diffusion technique from acetone and ether. An infrared spectrum (Beckman IR-8) in acetonitrile solution displayed one strong nitrosyl absorption band at 1720 cm^{-1}.

An X-ray crystallographic analysis of $[Co(\eta^5\text{-}C_5H_5)_2]^+[Fe_4(NO)_4(\mu_3\text{-}S)_4]^-$ was carried out, but the detailed crystal structure was not determined, presumably due to a crystal twinning and/or disorder apparently involving the cobaltocenium cations. Nevertheless, the crystallographic data and partial solution of the crystal structure established unambiguously the compound's stoichiometry. $[Co(\eta^5\text{-}C_5H_5)_2]^+[Fe_4(NO)_4(\mu_3\text{-}S)_4]^-$ crystallizes in a tetragonal unit cell with lattice constants, obtained from a Syntex $P\bar{1}$ diffractometer at ca. 22 °C, of $a = b = 17.343$ (9) Å and $c = 13.272$ (4) Å; the unit-cell volume is 3986 (3) $Å^3$. The observed density of 2.20 ± 0.02 g/cm^3, measured by the flotation method, is in excellent agreement with the calculated density of 2.20 g/cm^3 for $Z = 8$.

$[AsPh_4]^+[Fe_4(NO)_4(\mu_3\text{-}S)_4]^-$. The isolation of this salt was finally achieved in one experiment that involved (1) reduction with Na/Hg amalgam of the neutral compound in THF at room temperature followed by filtration of the product, (2) addition of an acetone solution of tetraphenylarsonium chloride to the filtrate to give a residue that was washed with hexane and then toluene to purge impurities from the insoluble ionic product, (3) extraction of the residue with acetone followed by a slow recrystallization of the vacuum-dried sample by solvent diffusion from an acetone–ether mixture under argon. Infrared spectra (Digilab FTS-20 spectrometer with 4.0 cm^{-1} resolution) of the resulting black crystalline material exhibited one sharp nitrosyl stretching frequency at 1700 cm^{-1} in the solid state (KBr pellet) and at 1725 cm^{-1} in CH_2Cl_2 solution.

Crystals of this compound were found from the X-ray diffraction investigation to possess a centrosymmetric orthorhombic cell with $a = 10.390$ Å, $b = 21.666$ Å, $c = 44.850$ Å, and $V = 10034$ $Å^3$. Our inability to obtain the complete crystal structure was at first thought to be a consequence of the extremely long c axis causing problems in a room-temperature data collection via the θ–2θ scan mode with Mo Kα radiation. A low-temperature ω-scan data set was then obtained, but an analysis of the data indicated that the difficultly in solving the entire structure could be ascribed to a crystal twinning and/or crystal disorder.

$[K(2,2,2\text{-crypt})]^+[Fe_4(NO)_4(\mu_3\text{-}S)_4]^-$. $Fe_4NO)_4(\mu_3\text{-}S)_4$ (0.56 g, 1.2 mmol) was dissolved in 40 mL of toluene in a 250-mL side-arm flask to which 2,2,2-cryptand (0.44 g, 1.2 mmol) was added. Benzophenone (0.22 g, 1.2 mmol) was dissolved in 30 mL of toluene in a Schlenk tube, and excess potassium metal was added to the benzophenone solution. This potassium/benzophenone solution was stirred for an hour; the color of the solution quickly turned from dark green to deep purple. The deep purple solution was filtered into the $Fe_4(NO)_4(\mu_3\text{-}S)_4$–cryptand solution. A shiny black precipitate was obtained. After being stirred for approximately 1 h, the solution was filtered and the filtrate washed with toluene. The precipitate was then dissolved in CH_2Cl_2; a slow diffusion of hexane into the CH_2Cl_2 solution of the $[K(2,2,2\text{-crypt})]^+[Fe_4(NO)_4(\mu_3\text{-}S)_4]^-$ produced suitable single crystals for an X-ray diffraction study. This ionic compound in crystalline form is reasonably stable in air but in solution it decomposes readily. It is soluble in CH_2Cl_2, THF, and acetonitrile but is insoluble in nonpolar solvents.

Infrared spectra of $[K(2,2,2\text{-crypt})]^+[Fe_4(NO)_4(\mu_3\text{-}S)_4]^-$ in solution and in the solid state (recorded on either a FTS-20 Fourier transform spectrophotometer or a Beckman Model 4240 spectrophotometer) are presented in Figure 1. As is typical in other nitrosyl metal clusters, the solution spectrum exhibits an intense but broad absorption band at 1730 cm^{-1} with several weak but unresolvable shoulders on both sides of the maximum absorption band. A KBr pellet spectrum exhibits a broad nitrosyl stretching band with the maximum at 1706 cm^{-1}. At least three bands are discernible, at 1706 (s), 1735 (s), and 1755 (m) cm^{-1}, with possibly a fourth peak (which is not as distinct) at 1718 (s) cm^{-1}. A Nujol mull spectrum was found to be similar to the KBr pellet spectrum, with maxima for three bands measured at 1712 (s), 1740 (s), and 1755 (m) cm^{-1}.

An ^{57}Fe Mössbauer spectrum of a polycrystalline sample of the $[K(2,2,2\text{-crypt})]^+[Fe_4(NO)_4(\mu_3\text{-}S)_4]^-$ was measured with a source of ^{57}Co at room temperature and zero applied field. A 0.2-g sample containing ca. 50 mg of iron metal was ground and dispersed evenly on the sample holder of 2.5-cm diameter and 1-mm thickness.

The magnetic susceptibility of $[K(2,2,2\text{-crypt})]^+[Fe_4(NO)_4(\mu_3\text{-}S)_4]^-$ in the crystalline state was determined at room temperature by the Faraday method with a quartz microbalance. Measurements were made at five different field strengths which varied from 5.92 to 7.90 kG. The molar susceptibility values corrected for the diamagnetism of the ligands were independent of the field strength, with a typical value being 1.56 × 10^{-3} cgs/mol. The corresponding magnetic moment of 1.92 μ_B is in accordance with that expected for one unpaired electron in the monoanion.

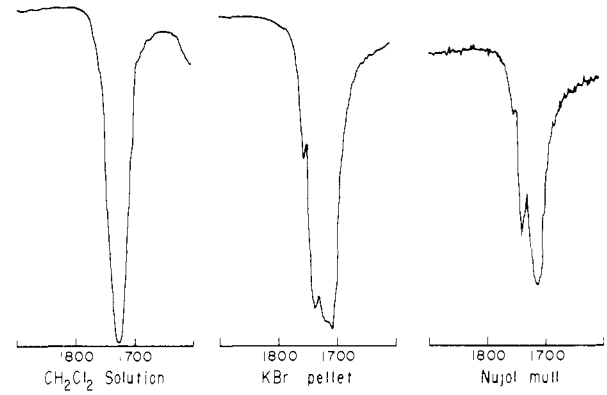

Figure 1. Solution and solid-state spectra of $[K(2,2,2\text{-crypt})]^+[Fe_4(NO)_4(\mu_4\text{-}S)_4]^-$ in the terminal nitrosyl stretching region. In contrast to the one intense broad absorption band observed in CH_2Cl_2 and other solution spectra, both the KBr pellet and Nujol mull spectra exhibit three discernible nitrosyl bands in accordance with its crystal structure displaying a specific cation–anion interaction involving one nitrosyl oxygen becoming part of the coordination polyhedron about the potassium ion.

X-ray Diffraction Analyses and Structural Refinements. $Fe_4(NO)_4(\mu_3\text{-}S)_4$. A parallelepiped-shaped crystal of dimensions 0.52 × 0.34 × 0.16 mm along the [101], [$\bar{1}$11], and [11$\bar{1}$] directions, respectively, was wedged into a thin-walled, argon-filled Lindemann glass capillary, which was then hermetically sealed. The capillary was glued with epoxy cement to a fiber such that the a axis was parallel to the goniometer spindle axis. Preliminary oscillation and Weissenberg photographs showed monoclinic C_{2h}–$2/m$ Laue symmetry.

The crystal was optically aligned and then centered with Mo Kα radiation on a Syntex $P\bar{1}$ diffractometer. The θ–2θ scan technique was utilized with stationary crystal–stationary counter background counting at both extremes of each scan and with variable scan speeds ranging from 3.0 to 24.0°/min. The scan speeds and widths for individual diffraction maxima were determined by relative peak intensities, and the ratio of total background counting time to scan time was 0.667. Two standard reflections, periodically measured every 48 reflections, showed no significant deviations in their intensities during the entire data collection. The intensities of two independent reciprocal lattice octants of data (viz., hkl and $hk\bar{l}$) were sampled once for the range $3.0° \leq 2\theta \leq 45.0°$. Data reduction[20a,b] yielded 1384 independent diffraction maxima with $I \geq 2\sigma(I)$. An analytical absorption correction[20c] was applied to the intensities in that the calculated transmission coefficients (based on a calculated linear absorption coefficient of 54.70 cm^{-1} for Mo Kα radiation) varied from 0.181 to 0.430.

The measured lattice constants at ca. 22 °C for the monoclinic cell are $a = 12.350$ (3) Å, $b = 9.627$ (7) Å, $c = 10.407$ (4) Å, and $\beta = 103.66$

(20) (a) Calabrese, J. C. "FOBS, a Fortran Diffractometer Data Reduction Program"; University of Wisconsin—Madison: Madison, WI, 1972. (b) Calabrese, J. C. SORTMERGE, Ph.D. Thesis, Univesity of Wisconsin—Madison, Madison, WI, 1971; Appendix. (c) Blount, J. F. "DEAR, A FORTRAN Absorption-Correction Program", 1965, based on the method given by: Busing, W. R.; Levy, H. A. *Acta Crystallogr.* **1957**, *10*, 180–182. (d) Calabrese, J. C. "MAP, a FORTRAN Summation and Molecular Assemblage Program", University of Wisconsin—Madison, Madison, WI, 1972. (e) Main, P.; Lessinger, L.; Woolfson, M. M.; Germain, G.; Declercq, J.-P. MULTAN-76, an undated version of MULTAN: Germain, G.; Main, P.; Woolfson, M. M. *Acta Crystallogr. Sect. A* **1971**, *A2*, 368–376. (f) "OR FLSR, A Local Rigid-Body Least-Squares Program", adapted from the Busing–Martin–Levy ORFLS: Report ORNL-TM-305; Oak Ridge National Laboratory, Oak Ridge, TN, 1962. (g) Busing, W. R.; Martin, K. O.; Levy, H. A. "OR FFE, A Fortran Crystallographic Function and Error Program"; Report ORNL-TM-306, Oak Ridge National Laboratory, Oak Ridge, TN, 1964. PLANES, a revised version of PLANES 1 written by: Smith, D. L. Ph.D. Thesis, University of Wisconsin—Madison, Madison, WI, 1962, Appendix IV. (i) Johnson, C. K. "OR TEP-II, A Fortran Thermal-Ellipsoid Plot Program for Crystal Structure Illustrations"; Report ORNL-5138, Oak Ridge National Laboratory, Oak Ridge, TN, 1976. (j) Broach, R. W. "Caress, a Fortran Program for the Computer Analysis of Step-Scan Data"; Ph.D. Thesis, University of Wisconsin—Madison, Madison, WI, 1977, Appendix I. (k) Broach, R. W. "QUICKSAM, A Fortran Program for Sorting and Merging Structure Factor Data"; Ph.D. Thesis, University of Wisconsin—Madison, Madison, WI, 1977, Appendix II. (l) Calabrese, J. C. "A Crystallographic Variable Matrix Least-Squares Refinement Program"; University of Wisconsin—Madison, Madison, WI, 1972. (m) Calabrese, J. C. MIRAGE, Ph.D. Thesis, University of Wisconsin—Madison, Madison WI, 1971, Appendix III.

Table I. Atomic Parameters for $Fe_4(NO)_4(\mu_3\text{-}S)_4$[a,b]

atom	x	y	z	$10^4\beta_{11}$	$10^4\beta_{22}$	$10^4\beta_{33}$	$10^4\beta_{12}$	$10^4\beta_{13}$	$10^4\beta_{23}$
Fe(1)	0.1037 (1)	0.2845 (1)	0.1038 (1)	53 (1)	104 (1)	98 (1)	9 (1)	26 (1)	7 (1)
Fe(2)	0.0441 (1)	0.0955 (1)	0.2577 (1)	65 (1)	89 (1)	86 (1)	8 (1)	20 (1)	2 (1)
Fe(3)	−0.0841 (1)	0.3158 (1)	0.1834 (1)	44 (1)	96 (1)	78 (1)	5 (1)	11 (1)	−12 (1)
Fe(4)	0.1097 (1)	0.3454 (1)	0.3545 (1)	54 (1)	107 (1)	92 (1)	10 (1)	−1 (1)	−20 (1)
S(1)	−0.0463 (1)	0.1510 (1)	0.0530 (1)	64 (1)	104 (2)	81 (2)	3 (1)	14 (1)	−21 (1)
S(2)	0.2125 (1)	0.1877 (2)	0.2817 (2)	49 (1)	122 (2)	119 (2)	21 (1)	12 (1)	2 (2)
S(3)	−0.0356 (1)	0.2259 (2)	0.3846 (2)	71 (1)	134 (2)	81 (2)	9 (1)	28 (1)	−3 (1)
S(4)	0.0429 (1)	0.4778 (1)	0.1795 (2)	59 (1)	84 (2)	121 (2)	4 (1)	13 (1)	0 (1)
N(1)	0.1626 (4)	0.2995 (5)	−0.0235 (6)	73 (4)	140 (7)	148 (8)	26 (4)	49 (5)	28 (6)
N(2)	0.0451 (4)	−0.0744 (5)	0.2871 (5)	98 (4)	100 (7)	100 (6)	9 (4)	32 (4)	7 (5)
N(3)	−0.2154 (4)	0.3719 (5)	0.1453 (5)	54 (4)	135 (6)	100 (6)	4 (4)	7 (4)	−32 (5)
N(4)	0.1726 (4)	0.4345 (6)	0.4881 (6)	72 (4)	148 (7)	153 (8)	30 (4)	−11 (5)	−60 (7)
O(1)	0.1996 (6)	0.3074 (6)	−0.1170 (6)	147 (6)	236 (9)	211 (9)	36 (6)	126 (7)	35 (7)
O(2)	0.0452 (5)	−0.1919 (5)	0.3025 (5)	189 (7)	103 (7)	154 (7)	12 (5)	64 (5)	20 (5)
O(3)	−0.3074 (4)	0.4075 (6)	0.1227 (5)	54 (4)	230 (8)	189 (8)	32 (4)	2 (4)	−45 (6)
O(4)	0.2141 (5)	0.4965 (7)	0.5808 (6)	132 (6)	283 (11)	212 (10)	44 (6)	−46 (6)	−171 (9)

[a] Estimated standard deviations of last significant figures are given in parentheses. [b] Anisotropic thermal parameters of the form $\exp[-(\beta_{11}h^2 + \beta_{22}k^2 + \beta_{33}l^2 + 2\beta_{12}hk + 2\beta_{13}hl + 2\beta_{23}kl)]$ were used.

(3)°. The unit-cell volume of 1202.3 (8) Å^3 affords a calculated density of 2.59 g/cm^3 for $Z = 4$ and fw = 471.69.

Systematic absences of $(h0l)$ for $h + l = 2n + 1$ and $(0k0)$ for $k = 2n + 1$ uniquely indicate the probable space group $P2_1/n$, which was confirmed by the structural determination and successful refinement. For this centrosymmetric space group the crystallographically independent unit contains four iron, four sulfur, four nitrogen, and four oxygen atoms (of one molecule) with each atom occupying the 4-fold set of general positions $\pm(x, y, z; {}^1/_2 + x, {}^1/_2 - y, {}^1/_2 + z)$.

The application of MULTAN[20e] followed by Fourier difference maps[20d] led to the solution of the crystal structure. Full-matrix least-squares refinement[20f] eventually converged at $R_1(F) = 3.2\%$ and $R_2(F) = 4.2\%$[21-24] with anisotropic thermal parameters utilized for all atoms (for which the data-to-parameter ratio was 9.5:1). A final difference Fourier map, which showed the largest peak to be less than 0.5 e/Å^3, revealed no anomalous features.

The positional and thermal parameters from the output of the final full-matrix least-squares cycle are given in Table I. Intramolecular distances and bond angles with estimated standard deviations calculated from the variance–covariance matrix[20g] are presented in Table II.[25] Selected least-squares planes[20h] of specified atoms were computed along with the perpendicular distances of these and other atoms from these planes and the angles between the normals to these planes. All illustrations were drawn with the aid of ORTEP.[20i]

$[K(2,2,2\text{-crypt})]^+[Fe_4(NO)_4(\mu_3\text{-}S)_4]^-$. A black needle-shaped crystal of dimensions 0.64 × 0.32 × 0.12 mm was chosen and mounted inside a thin-walled Lindemann glass capillary, which was evacuated, filled with argon, and then hermetically sealed. After optical alignment, the crystal was centered with Mo Kα radiation on a Syntex P$\bar{1}$ diffractometer and was determined to possess triclinic symmetry (which was substantiated by axial photographs). The lattice constants for the chosen unit cell at 23 °C are $a = 12.766$ (4) Å, $b = 13.118$ (4) Å, $c = 10.172$ (3) Å, $\alpha = 95.96$ (2)°, $\beta = 93.70$ (2)°, and $\gamma = 85.68$ (2)°; the unit-cell volume of 1686.6 (8) Å^3 gives rise to a calculated density of 1.75 g/cm^3 for $Z = 2$ and fw = 887.29.

Intensity data for four reciprocal lattice octants were obtained by the θ–2θ scan mode over a 2θ range of 3.0–50.0° with variable scan speeds of 4.0–24.0°. No significant changes in the intensities of the two standard reflections, sampled at intervals of 96 reflections, were observed during the data collection. The measured intensities of 6269 reflections yielded (after reduction[20j] and merging[20k]) 5973 independent data, of which the 4526 reflections with $I > 2\sigma(I)$ were used in the structural

Table II. Intramolecular Distances and Bond Angles for $Fe_4(NO)_4(\mu_3\text{-}S)_4$

Distances (Å) Averaged under Assumed T_d Symmetry			
Fe(1)-Fe(2)	2.641 (1)	Fe(1)-S(1)	2.213 (2)
Fe(1)-Fe(3)	2.658 (1)	Fe(1)-S(2)	2.219 (2)
Fe(1)-Fe(4)	2.657 (1)	Fe(1)-S(4)	2.220 (2)
Fe(2)-Fe(3)	2.650 (1)	Fe(2)-S(1)	2.224 (2)
Fe(2)-Fe(4)	2.659 (1)	Fe(2)-S(2)	2.221 (2)
Fe(3)-Fe(4)	2.640 (1)	Fe(2)-S(3)	2.214 (2)
		Fe(3)-S(1)	2.208 (1)
Fe(1)-N(1)	1.661 (5)	Fe(3)-S(3)	2.214 (2)
Fe(2)-N(2)	1.663 (5)	Fe(3)-S(4)	2.219 (2)
Fe(3)-N(3)	1.666 (5)	Fe(4)-S(2)	2.223 (2)
Fe(4)-N(4)	1.662 (6)	Fe(4)-S(3)	2.215 (2)
	1.663 (av)	Fe(4)-S(4)	2.217 (2)
			2.217 (av)
N(1)-O(1)	1.148 (7)		
N(2)-O(2)	1.143 (6)		
N(3)-O(3)	1.157 (6)	S(1)···S(2)	3.522 (2)
N(4)-O(4)	1.171 (6)	S(1)···S(3)	3.497 (2)
		S(1)···S(4)	3.487 (2)
	1.155 (av)	S(2)···S(3)	3.496 (2)
		S(2)···S(4)	3.503 (2)
		S(3)···S(4)	3.515 (2)
			3.503 (av)

B. Bond Angles (Deg) Averaged under Assumed T_d Symmetry			
Fe(1)-S(1)-Fe(2)	73.06 (5)	S(1)-Fe(1)-N(1)	111.0 (2)
Fe(1)-S(1)-Fe(3)	73.90 (5)	S(2)-Fe(1)-N(1)	114.2 (2)
Fe(2)-S(1)-Fe(3)	73.46 (5)	S(4)-Fe(1)-N(1)	117.3 (2)
Fe(1)-S(2)-Fe(2)	73.00 (5)	S(1)-Fe(2)-N(2)	113.1 (2)
Fe(1)-S(2)-Fe(4)	73.48 (5)	S(2)-Fe(2)-N(2)	114.0 (2)
Fe(2)-S(2)-Fe(4)	73.52 (5)	S(3)-Fe(2)-N(2)	115.7 (2)
Fe(2)-S(3)-Fe(3)	73.53 (5)	S(1)-Fe(3)-N(3)	115.0 (3)
Fe(2)-S(3)-Fe(4)	73.81 (5)	S(3)-Fe(3)-N(3)	112.5 (2)
Fe(3)-S(3)-Fe(4)	73.18 (6)	S(4)-Fe(3)-N(3)	114.8 (2)
Fe(1)-S(4)-Fe(3)	73.57 (5)	S(2)-Fe(4)-N(4)	116.5 (2)
Fe(1)-S(4)-Fe(4)	73.60 (5)	S(3)-Fe(4)-N(4)	112.5 (2)
Fe(3)-S(4)-Fe(4)	73.04 (5)	S(4)-Fe(4)-N(4)	113.6 (2)
	73.43 (av)		114.2 (av)
S(1)-Fe(1)-S(2)	105.23 (6)	Fe(1)-N(1)-O(1)	176.9 (5)
S(1)-Fe(1)-S(4)	103.73 (6)	Fe(2)-N(2)-O(2)	177.6 (5)
S(2)-Fe(1)-S(4)	104.20 (7)	Fe(3)-N(3)-O(3)	177.3 (5)
S(1)-Fe(2)-S(2)	104.84 (6)	Fe(4)-N(4)-O(4)	178.8 (5)
S(1)-Fe(2)-S(3)	104.01 (6)		177.6 (av)
S(2)-Fe(2)-S(3)	104.04 (7)		
S(1)-Fe(3)-S(3)	104.54 (6)		
S(1)-Fe(3)-S(4)	103.92 (6)		
S(3)-Fe(3)-S(4)	104.92 (7)		
S(2)-Fe(4)-S(3)	103.92 (7)		
S(2)-Fe(4)-S(4)	104.16 (7)		
S(3)-Fe(4)-S(4)	104.94 (6)		
	104.37 (av)		

(21) The unweighted and weighted discrepancy factors used are $R_1(F) = [\sum||F_o| - |F_c||/\sum|F_o|]100$ and $R_2(F) = [\sum w_i||F_o| - |F_c||^2/\sum w_i|F_o|^2]^{1/2}100$. All least-squares refinements were based on the minimization of $\sum w_i||F_o| - |F_c||^2$ with individual weights of $w_i = 1/\sigma^2(F_o)$ assigned on the basis of the esd's of the observed structure factors.

(22) The scattering factor tables used are those of Cromer and Mann[23a] for the nonhydrogen atoms and those of Stewart et al.[23b] for the hydrogen atoms. Real and imaginary corrections for anomalous dispersion (viz., $\Delta f' = 0.4$, $\Delta f'' = 1.0$ for Fe; $\Delta f' = 0.1$, $\Delta f'' = 0.2$ for S)[24] were included in the structure factor calculations.

(23) (a) Cromer, D. T.; Mann, J. B. *Acta Crystallogr., Sect. A* **1968**, *A24*, 321–324. (b) Stewart, R. F.; Davidson, E. R.; Simpson, W. T. *J. Chem. Phys.* **1965**, *42*, 3175–3187.

(24) "International Tables for X-Ray Crystallography"; Kynoch Press: Birmingham, England, 1974; Vol. IV, p 149.

(25) A listing of the observed and calculated structure factors is available without charge) upon request from the inorganic secretary, Department of Chemistry, University of Wisconsin—Madison, Madison, WI 53706.

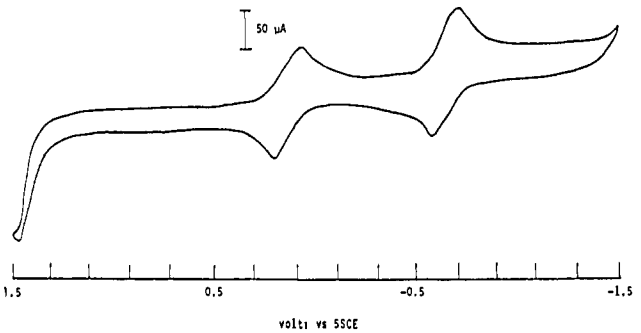

Figure 2. A 100 mV/s cyclic voltammogram of $Fe_4(NO)_4(\mu_3\text{-}S)_4$ (abbreviated as $[Fe_4S_4]^0$) in 0.1 M TBAH–CH_2Cl_2 solution at a platinum bead electrode displaying a chemically reversible, one-electron couple $[Fe_4S_4]^0/[Fe_4S_4]^-$ at $E_{1/2}$ = +0.13 V (vs. SCE) and a chemically reversible, one-electron couple $[Fe_4S_4]^-/[Fe_4S_4]^{2-}$ at $E_{1/2}$ = −0.65 V (vs. SCE).

determination and least-squares refinement. An analytical absorption correction[20c] was applied to the data in that the transmission coefficients, based upon a calculated linear absorption coefficient of 21.4 cm^{-1} for Mo Kα radiation, varied from 0.64 to 0.84.

An interpretation of a computed Patterson map provided tentative positions for four iron and three sulfur atoms with a geometrical arrangement consistent with an Fe_4S_4 cubane core. A Fourier synthesis phased on these seven atoms (with one atom arbitrarily placed at the origin) was calculated under noncentrosymmetric $P1$ symmetry. This map revealed not only the position of the remaining sulfur atom but also the atomic coordinates for a second Fe_4S_4 core related to the first one by a center of symmetry. The origin of the unit cell was then shifted to this calculated center of symmetry, and another Fourier map phased on the coordinates of one of the Fe_4S_4 cores was computed under centrosymmetric $P\bar{1}$ symmetry. This map exhibited peaks for all of the nonhydrogen atoms of $[K(2,2,2\text{-crypt})]^+[Fe_4(NO)_4(\mu_3\text{-}S)_4]^-$ except for two carbon atoms. A subsequent difference Fourier map located all nonhydrogen atoms. Least-squares refinement[20l] with individual isotropic temperature factors converged at $R_1(F)$ = 10.75% and $R_2(F)$ = 12.57%.[21-24] Idealized tetrahedral coordinates for the two hydrogen atoms of each methylene carbon atom in the 2,2,2-cryptand ligand were then calculated.[20m] Further least-squares refinement[20f] was carried out with varying positional and anisotropic thermal parameters for the nonhydrogen atoms and with fixed positional and isotropic thermal parameters for the hydrogen atoms. After each cycle of full-matrix least-squares refinement,[20f] new idealized tetrahedral coordinates for each hydrogen atom were calculated[20m] on the basis of the new carbon positions. The final cycle of the full-matrix least-squares refinement converged to $R_1(F)$ = 4.57% and $R_2(F)$ = 5.75%. The data-to-parameter ratio was 11.7:1, and the error of fit was 1.32. A final difference Fourier map showed no unusual features.

The atomic parameters from the output of the final least-squares cycle are given in Table III, while interatomic distances and bond angles[20g] are presented in Table IV.[25] Selected least-squares planes[20h] and interplanar angles were again calculated. ORTEP[20i] was used to draw all illustrations.

Results and Discussion

Electrochemical Properties. A 100 mV/s cyclic voltammogram of $Fe_4(NO)_4(\mu_3\text{-}S)_4$ in CH_2Cl_2 solution (Figure 2) indicates two chemically reversible couples, characteristic of two one-electron reductions of the neutral parent to the monoanion (n = 1−) and dianion (n = 2−).[16,26,27] The $E_{1/2}$ values (relative to SCE) relating to the various species in 0.1 M TBAH CH_2Cl_2 solution at 22 ± 2 °C at a platinum electrode, where $[Fe_4S_4]^n$ is an abbreviation for $[Fe_4(NO)_4(\mu_3\text{-}S)_4]^n$, are as follows: $[Fe_4S_4]^0$ 0.13 V $[Fe_4S_4]^-$ −0.65 V $[Fe_4S_4]^{2-}$.

The indicated chemical reversibility of these electron-transfer processes is based on the symmetrical appearance of the current–potential curves and the approximate equivalence of the anodic and cathodic peak currents. Although the measured separation of 135 ± 5 mV between the anodic and cathodic peaks for each of the two couples is considerably higher than the theoretical value of 57 mV required for an electrochemically reversible process, similar discrepancies from ideal behavior for known reversible couples have been observed in studies of other organometallic complexes.[28]

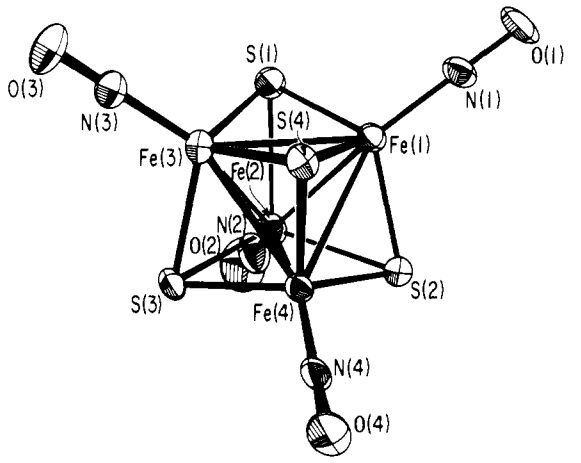

Figure 3. Cubanelike $Fe_4(NO)_4(\mu_3\text{-}S)_4$ molecule, which experimentally possesses cubic T_d symmetry with the Fe_4S_4 core containing a completely bonding iron tetrahedron.

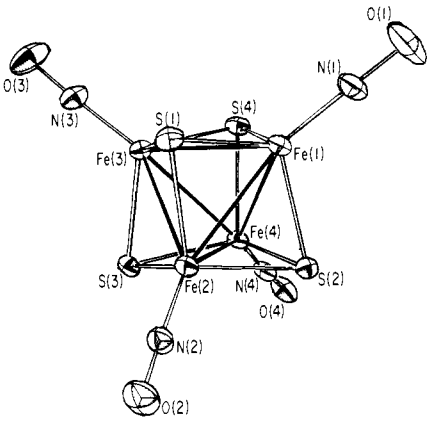

Figure 4. A view of the $[Fe_4(NO)_4(\mu_3\text{-}S)_4]^-$ monoanion, which has an idealized tetragonal D_{2d} configuration with no crystallographically required symmetry.

General Description of the Crystal and Molecular Structure of $Fe_4(NO)_4(\mu_3\text{-}S)_4$. The molecular configuration of $Fe_4(NO)_4(\mu_3\text{-}S)_4$ possesses a cubanelike framework with the four triply bridging sulfur ligands situated above the four triangular faces of the iron tetrahedron such that the iron and sulfur atoms occupy alternate corners of a distorted cube (Figure 3). The molecule, which has no imposed crystallographic constraints, complies almost exactly with cubic T_d symmetry. The closest intermolecular O···O distances of 3.2 Å do not indicate any unusual intermolecular interactions.

The iron atoms form a completely bonding tetrahedron of average length 2.651 Å. The 12 chemically equivalent Fe–S bond lengths vary from only 2.208 (1) to 2.224 (2) Å, with a mean of 2.217 Å. The four Fe–NO bond lengths vary from only 1.661 (5) to 1.666 (5) Å, with a mean of 1.663 Å, while the four N–O bond lengths are of the range 1.143 (6)–1.171 (6) Å, with a mean

(26) A value of n = 0.7 (corresponding to a one-electron transfer) was calculated for each of the two waves from the equation $i = nFAD_0^{1/2}C_0^*a^{1/2}[\pi^{1/2}\chi(at)]$,[27] where i = peak current (48 × 10^{-6} A), F = 96 500 Coulombs, A = area of electrode = $4\pi r^2$ (r = 1.6 mm), D_0 = diffusion coefficient (~1.7 × 10^{-5} cm^2/s for CH_2Cl_2), C_0^* = bulk concentration (6.35 × 10^{-7} mole/cm^3), a = (nFV/RT), where V = scan rate (100 mV/s), R = 8.31 × 10^7 erg deg^{-1} mol^{-1}, T = 298 K, and $[\pi^{1/2}\chi(at)]$ = current function ≈0.446.

(27) Nicholson, R. S.; Shain, I. *Anal. Chem.* **1964**, *36*, 706–723.

(28) See: (a) Kotz, J. C.; Nivert, C. L. Lieber, J. M.; Reed, R. C. *J. Organomet. Chem.* **1975**, *91*, 87–95. (b) Lloyd, M. K.; McCleverty, J. A.; Orchard, D. G.; Connor, J. A.; Hall, M. B.; Hillier, I. H.; Jones, E. M.; McEwen, G. K., *J. Chem. Soc., Dalton Trans.* **1973**, *1743*–1747. (c) Morrison, W. H., Jr.; Kogsrud, S.; Hendrickson, D. N. *Inorg. Chem.* **1973**, *12*, 1998–2004.

Table III. Atomic Parameters for $[K(2,2,2\text{-crypt})]^+[Fe_4(NO)_4(\mu_3\text{-}S)_4]^-$

Nonhydrogen Atoms[a]

atom	10^4x	10^4y	10^4z	10^4U_{11}	10^4U_{22}	10^4U_{33}	10^4U_{12}	10^4U_{13}	10^4U_{23}
Fe(1)	8029 (1)	159 (1)	453 (1)	292 (4)	342 (4)	504 (5)	−30 (3)	14 (3)	−34 (4)
Fe(2)	7260 (1)	−1008 (1)	−1684 (1)	359 (4)	368 (4)	432 (5)	−72 (3)	−44 (3)	56 (3)
Fe(3)	8732 (1)	−1816 (1)	2 (1)	293 (4)	365 (4)	445 (5)	19 (3)	15 (3)	41 (3)
Fe(4)	6748 (1)	−1325 (1)	751 (1)	283 (4)	432 (5)	497 (5)	−25 (3)	42 (3)	100 (4)
S(1)	8914 (1)	−556 (1)	−1265 (1)	344 (7)	397 (8)	500 (9)	−53 (6)	75 (6)	31 (6)
S(2)	6355 (1)	77 (1)	−286 (2)	287 (7)	394 (8)	638 (0)	20 (6)	−10 (6)	61 (7)
S(3)	7267 (1)	−2520 (1)	−852 (1)	441 (8)	335 (9)	550 (8)	−96 (6)	−33 (6)	43 (7)
S(4)	8248 (1)	−1001 (1)	1919 (2)	384 (8)	559 (7)	409 (9)	21 (6)	−24 (7)	18 (6)
N(1)	8313 (3)	1329 (4)	1089 (5)	338 (25)	428 (30)	733 (37)	−64 (21)	114 (24)	−82 (26)
N(2)	6784 (4)	−1018 (4)	−3238 (5)	676 (34)	513 (32)	481 (32)	−246 (26)	−113 (26)	158 (25)
N(3)	9740 (4)	−2684 (4)	150 (5)	419 (27)	493 (30)	477 (30)	89 (23)	55 (22)	105 (23)
N(4)	5801 (4)	−1652 (4)	1638 (6)	366 (27)	797 (40)	732 (39)	−4 (26)	81 (26)	318 (32)
O(1)	8480 (4)	2153 (3)	1564 (5)	663 (31)	517 (29)	1103 (42)	−295 (24)	322 (28)	−268 (28)
O(2)	6400 (5)	−1034 (4)	−4324 (5)	1447 (53)	1051 (45)	619 (35)	−640 (39)	−440 (35)	359 (31)
O(3)	10414 (4)	−3323 (4)	275 (5)	606 (29)	754 (33)	842 (36)	335 (26)	141 (25)	241 (28)
O(4)	5147 (4)	−1896 (6)	2259 (7)	677 (36)	1656 (64)	1563 (63)	7 (38)	532 (40)	821 (52)
K	7739 (1)	3569 (1)	4088 (1)	354 (6)	361 (6)	384 (7)	−38 (5)	29 (5)	35 (5)
N(11)	7390 (3)	5379 (3)	2502 (5)	458 (27)	377 (26)	460 (29)	−36 (21)	−43 (22)	103 (21)
C(12)	7347 (5)	6323 (4)	3440 (7)	710 (43)	304 (33)	735 (47)	−32 (29)	−50 (35)	133 (31)
C(13)	6616 (5)	6298 (5)	4533 (7)	626 (41)	413 (36)	723 (47)	115 (30)	50 (35)	−20 (32)
O(14)	6979 (3)	5520 (3)	5327 (4)	523 (24)	441 (24)	542 (26)	62 (19)	99 (20)	−18 (19)
C(15)	6308 (5)	5470 (5)	6386 (7)	526 (37)	604 (41)	557 (41)	16 (31)	132 (31)	−181 (33)
C(16)	6813 (5)	4764 (5)	7329 (6)	602 (40)	630 (42)	429 (36)	−111 (32)	102 (30)	−132 (31)
O(17)	6919 (3)	3752 (3)	6694 (4)	710 (29)	567 (27)	393 (24)	−69 (22)	106 (21)	−88 (21)
C(18)	7445 (7)	3060 (6)	7552 (7)	1124 (64)	811 (55)	386 (40)	88 (46)	155 (40)	58 (37)
C(19)	7450 (6)	1986 (6)	6883 (7)	1002 (57)	647 (47)	560 (44)	−34 (40)	292 (40)	203 (37)
N(20)	8092 (4)	1829 (4)	5725 (5)	564 (30)	479 (30)	438 (29)	−49 (23)	51 (23)	156 (23)
C(21)	9219 (5)	1677 (5)	6141 (6)	631 (41)	639 (44)	539 (40)	−51 (33)	−102 (32)	251 (33)
C(22)	9950 (5)	1782 (5)	5080 (7)	481 (36)	521 (39)	754 (48)	57 (29)	−23 (32)	139 (34)
O(23)	9874 (3)	2815 (3)	4756 (4)	423 (21)	476 (23)	464 (24)	36 (17)	47 (18)	65 (19)
C(24)	10531 (4)	2931 (5)	3725 (6)	373 (31)	598 (40)	552 (39)	−2 (27)	79 (28)	−34 (31)
C(25)	10474 (4)	4009 (5)	3412 (6)	301 (29)	697 (43)	583 (39)	−94 (28)	16 (26)	103 (32)
O(26)	9429 (3)	4292 (3)	2938 (4)	373 (21)	503 (24)	581 (26)	−118 (17)	16 (18)	222 (20)
C(27)	9344 (5)	5221 (5)	2350 (7)	486 (36)	589 (42)	791 (48)	−178 (31)	57 (33)	290 (36)
C(28)	8279 (5)	5362 (5)	1654 (6)	647 (41)	620 (42)	523 (39)	−66 (32)	70 (32)	260 (33)
C(29)	6412 (5)	5313 (5)	1681 (7)	583 (38)	454 (36)	646 (43)	2 (29)	−154 (32)	168 (31)
C(30)	6220 (5)	4238 (5)	1109 (6)	627 (39)	523 (38)	420 (36)	2 (30)	−146 (29)	69 (29)
O(31)	6034 (3)	3631 (3)	2129 (4)	431 (21)	397 (22)	433 (23)	−45 (17)	−33 (17)	−21 (17)
C(32)	5742 (4)	2640 (5)	1604 (6)	380 (31)	487 (36)	630 (41)	−82 (26)	−107 (28)	−101 (31)
C(33)	5654 (4)	1977 (5)	2685 (7)	372 (32)	462 (36)	771 (46)	−114 (26)	44 (30)	−47 (32)
O(34)	6657 (3)	1823 (3)	3354 (4)	391 (21)	417 (22)	610 (26)	−97 (17)	35 (18)	77 (19)
C(35)	6695 (5)	1025 (5)	4183 (7)	621 (41)	439 (36)	714 (45)	−168 (30)	83 (34)	75 (32)
C(36)	7787 (5)	909 (5)	4853 (7)	648 (41)	414 (35)	659 (43)	−90 (30)	31 (33)	156 (31)

Hydrogen Atoms[b]

atom	x	y	z	atom	x	y	z	atom	x	y	z
H(1)	7136	6934	2942	H(13)	9362	988	6477	H(25)	6420	5764	948
H(2)	8070	6452	3829	H(14)	9387	2173	6928	H(26)	5807	5600	2213
H(3)	5895	6163	4142	H(15)	9757	1315	4275	H(27)	6848	3932	632
H(4)	6587	6976	5083	H(16)	10689	1590	5400	H(28)	5595	4252	463
H(5)	5620	5215	6022	H(17)	10313	2478	2917	H(29)	6282	2316	992
H(6)	6182	6173	6859	H(18)	11274	2710	3994	H(30)	5053	2704	1086
H(7)	6370	4776	8107	H(19)	10974	4079	2715	H(31)	5405	1299	2302
H(8)	7524	4993	7645	H(20)	10662	4465	4230	H(32)	5143	2318	3324
H(9)	7070	3100	8391	H(21)	9899	5206	1695	H(33)	6536	367	3641
H(10)	8186	3250	7761	H(22)	9445	5806	3047	H(34)	6287	1255	4980
H(11)	6712	1815	6612	H(23)	8204	4813	903	H(35)	8315	732	4167
H(12)	7712	1489	7532	H(24)	8234	6006	1202	H(36)	7840	299	5374

[a] Anisotropic thermal parameters of the form $\exp[-2\pi^2(U_{11}h^2a^{*2} + U_{22}k^2b^{*2} + U_{33}l^2c^{*2} + 2U_{12}hka^*b^* + 2U_{13}hla^*c^* + 2U_{23}klb^*c^*)]$ were used. [b] The hydrogen atoms were assigned a fixed isotropic temperature factor of 8.0 Å^2. Their idealized fixed tetrahedral coordinates ($\times10^4$) are given.

of 1.155 Å. The nearly linear linkage of each nitrosyl ligand to its iron atoms, shown from the 176.9 (5)–178.8 (5)° range for the four Fe–N–O angles, is in accordance with the presumed absence of any electronically induced nitrosyl distortion[29] due to the localized C_{3v} environment about each iron atom.

General Description of the Crystal Structure of $[K(2,2,2\text{-crypt})]^+[Fe_4(NO)_4(\mu_3\text{-}S)_4]^-$. The one cation and one anion (Figure 4) constituting the crystallographically independent unit are found to form ion pairs in the solid state (Figure 5) due primarily to a short contact of 3.15 Å between the oxygen atom, O(1), of one nitrosyl ligand and the potassium ion; the other resulting shortest interionic separations are the O(1)···O(34) and O(1)···O(26) distances of 3.13 and 3.28 Å, respectively. Despite this particular ion-pair interaction, the structure of the Fe_4S_4 core of the $[Fe_4(NO)_4(\mu_3\text{-}S)_4]^-$ monoanion does not appear to be significantly distorted from its predicted tetragonal D_{2d}-$\bar{4}2m$ geometry (vide infra).

Geometrical Effects of the Solid-State Cation–Anion Interaction on the $[K(2,2,2\text{-crypt})]^+$ Cation and Resulting Implications. The

(29) Enemark, J. H. *Inorg. Chem.* **1971**, *10*, 1952–1957.

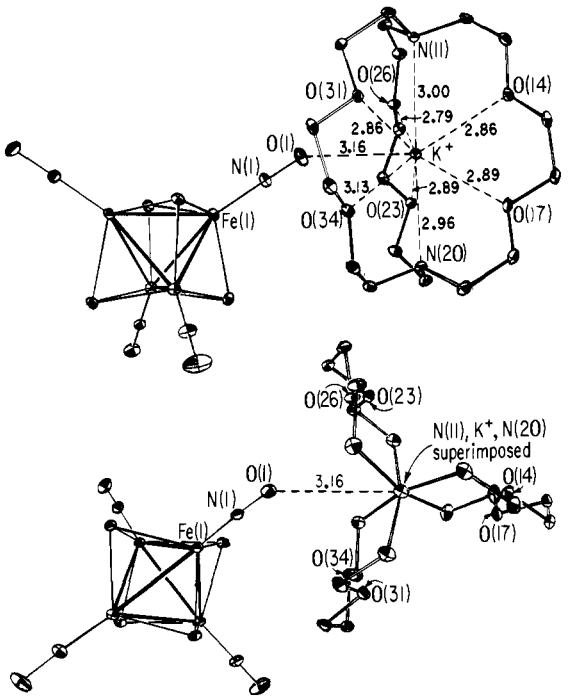

Figure 5. Two views revealing the spatial relationship in the specific ion-pair interaction of one nitrosyl oxygen, O(1), of the $[Fe_4(NO)_4(\mu_3\text{-}S)_4]^-$ monoanion with the K^+ ion of the $[K(2,2,2\text{-crypt})]^+$ monocation. The resulting nine-coordinated polyhedron of seven oxygen and two nitrogen atoms encapsulating the K^+ ion may be conceptually considered as a tricapped trigonal prism with the O(1) atom capping one of the three rectangular faces of the trigonal oxygen prism, which is capped on both trigonal faces by the two cryptand nitrogen atoms.

resulting nine-coordinated geometry of seven oxygen and two nitrogen atoms about the potassium ion in $[K(2,2,2\text{-crypt})]^+[Fe_4(NO)_4(\mu_3\text{-}S)_4]^-$ may be envisioned as a bicapped trigonal prism additionally capped by the nitrosyl oxygen atom on one of the three rectangular oxygen faces. This asymmetrical oxygen–nitrogen polyhedron about the potassium ion expectedly produces the following prominent structural variations upon comparison with the normal configuration of the $[K(2,2,2\text{-crypt})]^+$ monocation,[30] which was initially structurally analyzed by Weiss and colleagues[31] as the iodide salt and which subsequently has been structurally characterized several times by Corbett and co-workers[32] in their extensive utilization of it and the sodium analogue as gegenions to stablize a number of homopolyatomic anions: (1) There is a marked distortion of the trigonal array of cryptand oxygen atoms from 3-fold symmetry. The extent of this deformation is indicated by each of the two trigonal oxygen planes changing from an equilateral triangle in the iodide salt with an average O···O distance of 4.26 Å to an irregular triangle with significantly different distances (viz., 4.056 (5), 4.205 (5), and 4.491 (5) Å for one triangle and 4.032 (6), 4.403 (6), and 4.491 (5) Å for the other one), of which the longest edge in each triangle involves the two oxygen atoms adjacent to the nitrosyl O(1) atom (see Figure 5). (2) The mean K^+–O and K^+–N contacts are enlarged compared to the corresponding ones in $[K(2,2,2\text{-crypt})]^+I^-$. Whereas the six K^+–O(cryptand) distances in the iodide salt are all within 0.014 Å of the mean value of 2.785 Å, the K^+–O(34) distance of 3.127 (6) Å in the $[Fe_4(NO)_4(\mu_3\text{-}S)_4]^-$ salt is considerably longer than the other five K^+–O(cryptand) distances of range 2.790 (4)–2.893 (4) Å. The mean of 2.90 Å for the six K^+–O(cryptand) distances is 0.12 Å larger than that determined in the iodide salt. Moreover, the mean of 2.98 Å for the two K^+–N separations of 2.955 (5) and 2.997 (5) Å is 0.10 Å longer than that found in the iodide salt. These longer separations with a nine- rather than eight-coordinated polyhedron about the K^+ ion can be readily rationalized on the basis of smaller individual ion–dipole interactions coupled with increased steric effects. (3) There is a much closer conformity of the six cryptand oxygen atoms to a trigonal prism in the $[Fe_4(NO)_4(\mu_3\text{-}S)_4]^-$ salt, as evidenced by the average twist angle α[33] (11.1°) (the mean of 9.5, 11.1, and 12.7°) being much smaller than that (22.5°) in the iodide salt.

These considerable structural changes in the $[K(2,2,2\text{-crypt})]^+$ monocation due to the formation of ion pairing are in accordance with the general observation[34] that the cryptand ligand is very flexible in its dimensions when ions of different sizes and charges are embedded in its cavity. Although alkali metal cations have been conclusively shown from X-ray diffraction studies by Bau and co-workers[35] to form tight ion interactions with carbonyl oxygen atoms in mononuclear metal carbonyl anions, it is particularly noteworthy that $[K(2,2,2\text{-crypt})]^+[Fe_4(NO)_4(\mu_3\text{-}S)_4]^-$ is only the second solid-state example (to our knowledge) of an alkali metal ion surrounded by a 2,2,2-cryptand ligand that also interacts with the anion. This other example involves $[K(2,2,2\text{-crypt})]^+[Cr_2(CO)_{10}(\mu_2\text{-}H)]^-$, which was found from a combined room-temperature X-ray and low-temperature (20 K) neutron diffraction study by Petersen, Brown, and Williams[36] to possess one unusually short K^+–OC(eq) distance of 2.966 (3) Å, corresponding to an analogous polyhedral environment of seven oxygen and two nitrogen atoms surrounding the K^+ ion. However, for bivalent cations such as Ca^{2+}, Ba^{2+}, and Pb^{2+}, there are structural examples[37,38] that show that the 2,2,2-cryptand ligand cannot completely shield the bivalent ion from interacting with either the anion or solvent molecules (as observed in crystalline state) thereby resulting in high coordination numbers for the bivalent cation with the concomitant formation of ion pairs.

This observed crystalline interaction of one nitrosyl ligand of the anion with the cation in $[K(2,2,2\text{-crypt})]^+[Fe_4(NO)_4(\mu_3\text{-}S)_4]^-$ is consistent with its solid-state infrared spectra (Figure 1), which show at least three nitrosyl absorption bands, at 1710 (s), 1740 (s), and 1775 (m) cm^{-1} in Nujol mull and at 1706 (s), 1735 (s), and 1755 (m) cm^{-1} in KBr pellet form, as opposed to a solution spectrum, which shows only one strong broad peak at 1730 cm^{-1} (indicative that this cation–anion interaction is absent in solution). The most likely explanation for the solid-state infrared spectra exhibiting a complex nitrosyl absorption pattern is that the symmetry of the crystalline surroundings dominates over the local symmetry of the monoanion in determining the selection rules such that inactive bands become active and the degenerate vibrational bands are split. However, the presumed charge polarization of the nitrosyl ligand by the K^+ ion does not appear to alter significantly the geometry of the nitrosyl ligand relative to that of the other three nitrosyl ligands in that the corresponding Fe–NO and N–O bond lengths as well as Fe–N–O bond angles do not show any significant differences among one another. In conclusion, these results from the structural analysis are consistent with the premise that the cation–anion interaction is a distinct interaction that noticeably affects the nitrosyl IR frequencies but that apparently does not give rise to any pronounced geometrical perturbation of the $[Fe_4(NO)_4(\mu_3\text{-}S)_4]^-$ monoanion.

(30) It is noteworthy that stability constants of 2,2,2-cryptand with K^+ have been recently determined by potentiometric titration in methanol and in several aprotic, polar solvents at various temperatures (Gutknecht, J.; Schneider, H.; Stroka, J. *Inorg. Chem.* **1978**, *17*, 3326–3329).

(31) Moras, D.; Metz, B.; Weiss, R. *Acta Crystallogr., Sect. B* **1973**, *B29*, 383–388.

(32) (a) Cisar, A.; Corbett, J. D. *Inorg. Chem.* **1977**, *16*, 632–635. (b) Cisar, A.; Corbett, J. D. *Ibid.* **1977**, *16*, 2482–2487. (c) Belin, C. H. E.; Corbett, J. D.; Cisar, A. *J. Am. Chem. Soc.* **1977**, *99*, 7163–7169.

(33) This angle[31] denotes the extent of twisting between the two oxygen triangles (about the assumed 3-fold axis passing through the two nitrogen atoms) from an eclipsed trigonal prism (for $\alpha = 0°$) toward a trigonal antiprism (for $\alpha = 60°$).

(34) Lehn, J. M. *Acc. Chem. Res.* **1978**, *11*, 49–57.

(35) (a) Chin, H. B. Bau, R. *J. Am. Chem. Soc.* **1976**, *98*, 2434–2439. (b) Teller, R. G.; Finke, R. G.; Collman, J. P.; Chin, H. B.; Bau, R. *J. Am. Chem. Soc.* **1977**, *99*, 1104–1111.

(36) Petersen, J. L.; Brown, R. K., Williams, J. M. *Inorg. Chem.* **1981**, *20*, 158–165.

(37) Metz, B.; Weiss, R. *Inorg. Chem.* **1974**, *13*, 2094–2098.

(38) Metz, B.; Moras, D.; Weiss, R. *Acta Crystallogr., Sect. B* **1973**, *B29*, 1377–1381. *Ibid.* **1973**, *B29*, 1382–1387.

Table IV. Distances and Bond Angles for $[K(2,2,2\text{-crypt})]^+[Fe_4(NO)_4(\mu_3\text{-}S)_4]^-$

Intraanion Distances (Å) Averaged under Assumed D_{2d} Symmetry

Fe(1)-Fe(2)	2.703 (1)	S(1)···S(4)	3.519 (2)
Fe(3)-Fe(4)	2.704 (1)	S(1)···S(3)	3.520 (2)
	2.704 (av)	S(2)···S(4)	3.511 (2)
		S(2)···S(3)	3.519 (2)
Fe(1)-Fe(3)	2.682 (1)		3.517 (av)
Fe(1)-Fe(4)	2.690 (1)		
Fe(2)-Fe(3)	2.695 (1)	Fe(1)-S(4)	2.231 (2)
Fe(2)-Fe(4)	2.684 (1)	Fe(2)-S(3)	2.235 (2)
	2.688 (av)	Fe(3)-S(1)	2.234 (2)
		Fe(4)-S(2)	2.224 (2)
Fe(1)-N(1)	1.659 (5)		2.231 (av)
Fe(2)-N(2)	1.655 (5)		
Fe(3)-N(3)	1.663 (5)	Fe(1)-S(1)	2.230 (2)
Fe(4)-N(4)	1.660 (5)	Fe(1)-S(2)	2.227 (2)
	1.659 (av)	Fe(2)-S(1)	2.239 (2)
		Fe(2)-S(2)	2.221 (2)
N(1)-O(1)	1.167 (6)	Fe(3)-S(4)	2.224 (2)
N(2)-O(2)	1.178 (6)	Fe(3)-S(3)	2.234 (2)
N(3)-O(3)	1.166 (6)	Fe(4)-S(4)	2.233 (2)
N(4)-O(4)	1.162 (6)	Fe(4)-S(3)	2.239 (2)
	1.168 (av)		2.231 (av)
S(1)···S(2)	3.493 (2)		
S(3)···S(4)	3.499 (2)		
	3.496 (av)		

Intraanion Bond Angles (Deg) Averaged under Assumed D_{2d} Symmetry

Fe(3)-Fe(1)-Fe(4)	60.45 (3)	S(3)-S(1)-S(4)	59.61 (5)
Fe(3)-Fe(2)-Fe(4)	60.35 (3)	S(3)-S(2)-S(4)	59.71 (5)
Fe(1)-Fe(3)-Fe(2)	60.36 (4)	S(1)-S(3)-S(2)	59.50 (4)
Fe(1)-Fe(4)-Fe(2)	60.40 (3)	S(1)-S(4)-S(2)	59.58 (4)
	60.39 (av)		59.60 (av)
Fe(2)-Fe(1)-Fe(3)	60.06 (4)	S(2)-S(1)-S(3)	60.23 (5)
Fe(2)-Fe(1)-Fe(4)	59.71 (3)	S(2)-S(1)-S(4)	60.08 (5)
Fe(1)-Fe(2)-Fe(3)	59.58 (4)	S(1)-S(2)-S(3)	60.28 (4)
Fe(1)-Fe(2)-Fe(4)	59.89 (4)	S(1)-S(2)-S(4)	60.33 (4)
Fe(1)-Fe(3)-Fe(4)	59.91 (3)	S(1)-S(3)-S(4)	60.18 (5)
Fe(2)-Fe(3)-Fe(4)	59.63 (3)	S(2)-S(3)-S(4)	60.03 (5)
Fe(1)-Fe(4)-Fe(3)	59.63 (3)	S(1)-S(4)-S(3)	60.21 (5)
Fe(2)-Fe(4)-Fe(3)	60.02 (3)	S(2)-S(4)-S(3)	60.26 (5)
	59.80 (av)		60.20 (av)
S(1)-Fe(1)-S(2)	103.22 (7)	Fe(1)-S(1)-Fe(2)	74.43 (5)
S(1)-Fe(2)-S(2)	103.10 (6)	Fe(1)-S(2)-Fe(2)	74.85 (5)
S(3)-Fe(3)-S(4)	103.41 (7)	Fe(3)-S(3)-Fe(4)	74.39 (5)
S(3)-Fe(4)-S(4)	103.00 (6)	Fe(3)-S(4)-Fe(4)	74.69 (5)
	103.18 (av)		74.59 (av)
S(1)-Fe(1)-S(4)	104.16 (6)	Fe(1)-S(1)-Fe(3)	73.86 (6)
S(2)-Fe(1)-S(4)	103.90 (6)	Fe(2)-S(1)-Fe(3)	74.09 (5)
S(1)-Fe(2)-S(3)	103.77 (6)	Fe(1)-S(2)-Fe(4)	74.36 (6)
S(2)-Fe(2)-S(3)	104.31 (7)	Fe(2)-S(2)-Fe(4)	74.31 (6)
S(1)-Fe(3)-S(3)	104.00 (6)	Fe(2)-S(3)-Fe(3)	74.16 (5)
S(1)-Fe(3)-S(4)	104.26 (7)	Fe(2)-S(3)-Fe(4)	73.74 (6)
S(2)-Fe(4)-S(3)	104.09 (7)	Fe(1)-S(4)-Fe(3)	74.00 (5)
S(2)-Fe(4)-S(4)	103.95 (7)	Fe(1)-S(4)-Fe(4)	74.08 (6)
	104.06 (av)		74.08 (av)
Fe(1)-N(1)-O(1)	177.4 (4)		
Fe(2)-N(2)-O(2)	176.9 (5)		
Fe(3)-N(3)-O(3)	176.8 (5)		
Fe(4)-N(4)-O(4)	178.9 (6)		
	177.5 (av)		

Intracation Distances (Å)

K···N(11)	2.997 (5)	C(12)-C(13)	1.501 (9)
K···O(14)	2.862 (4)	C(15)-C(16)	1.487 (9)
K···O(17)	2.893 (4)	C(18)-C(19)	1.500 (10)
K···N(20)	2.955 (5)	C(21)-C(22)	1.495 (9)
K···O(23)	2.892 (4)	C(24)-C(25)	1.477 (9)
K···O(26)	2.790 (4)	C(27)-C(28)	1.500 (9)
K···O(31)	2.858 (4)	C(29)-C(30)	1.500 (8)
K···O(34)	3.127 (6)	C(32)-C(33)	1.486 (9)
		C(35)-C(36)	1.516 (9)
O(14)-C(13)	1.400 (8)		
O(14)-C(15)	1.429 (7)	N(11)···O(14)	2.938 (6)
O(17)-C(16)	1.415 (7)	N(11)···O(26)	2.904 (6)
O(17)-C(18)	1.426 (8)	N(11)···O(31)	2.955 (6)
O(23)-C(22)	1.423 (7)	N(20)···O(17)	2.948 (7)
O(23)-C(24)	1.412 (7)	N(20)···O(23)	2.970 (6)
O(26)-C(25)	1.425 (6)	N(20)···O(34)	2.933 (6)
O(26)-C(27)	1.406 (7)	O(14)···O(17)	2.834 (6)
O(31)-C(30)	1.413 (7)	O(26)···O(23)	2.818 (5)
O(31)-C(32)	1.420 (6)	O(31)···O(34)	2.831 (5)
O(34)-C(33)	1.421 (7)		
O(34)-C(35)	1.407 (7)	O(14)···O(26)	4.205 (4)
		O(14)···O(31)	4.056 (5)
N(11)-C(12)	1.483 (8)	O(31)···O(26)	4.491 (5)
N(11)-C(28)	1.466 (7)	O(17)···O(23)	4.403 (6)
N(11)-C(29)	1.459 (7)	O(17)···O(34)	4.032 (6)
N(20)-C(19)	1.466 (8)	O(23)···O(34)	4.501 (5)
N(20)-C(21)	1.478 (8)		
N(20)-C(36)	1.483 (8)		

Intracation Angles (Deg)

N(11)-K-N(20)	178.3 (1)	C(12)-N(11)-C(28)	110.6 (5)
N(11)-K-O(14)	60.1 (1)	C(12)-N(11)-C(29)	110.7 (5)
N(11)-K-O(26)	60.1 (1)	C(28)-N(11)-C(29)	109.6 (5)
N(11)-K-O(31)	60.6 (1)	C(19)-N(20)-C(21)	110.5 (5)
N(11)-K-O(17)	118.1 (1)	C(19)-N(20)-C(36)	110.4 (5)
N(11)-K-O(23)	118.8 (1)	C(21)-N(20)-C(36)	108.5 (5)
N(11)-K-O(34)	120.0 (1)	N(11)-C(12)-C(13)	114.0 (5)
N(20)-K-O(17)	60.5 (1)	C(12)-C(13)-O(14)	109.6 (5)
N(20)-K-O(23)	61.1 (1)	C(13)-O(14)-C(15)	111.6 (5)
N(20)-K-O(34)	105.1 (1)	O(14)-C(15)-C(16)	109.7 (5)
N(20)-K-O(14)	118.3 (1)	C(15)-C(16)-O(17)	109.8 (5)
N(20)-K-O(26)	120.0 (1)	C(16)-O(17)-C(18)	111.4 (5)
N(20)-K-O(31)	120.6 (1)	O(17)-C(18)-C(19)	109.4 (6)
O(14)-K-O(17)	59.0 (1)	C(18)-C(19)-N(20)	113.0 (6)
O(26)-K-O(23)	59.5 (1)	N(20)-C(21)-C(22)	114.2 (5)
O(31)-K-O(34)	60.3 (1)	C(21)-C(22)-O(23)	109.7 (5)
O(14)-K-O(26)	92.2 (1)	C(22)-O(23)-C(24)	111.0 (4)
O(14)-K-O(31)	90.3 (1)	O(23)-C(24)-C(25)	111.0 (5)
O(26)-K-O(31)	105.4 (1)	C(24)-C(25)-O(26)	109.0 (5)
O(17)-K-O(23)	99.1 (1)	C(25)-O(26)-C(27)	113.2 (4)
O(17)-K-O(34)	90.7 (1)	O(26)-C(27)-C(28)	109.8 (5)
O(23)-K-O(34)	105.1 (1)	C(27)-C(28)-N(11)	115.0 (5)
O(14)-K-O(23)	118.5 (1)	N(11)-C(29)-C(30)	113.2 (5)
O(14)-K-O(34)	129.0 (1)	C(29)-C(30)-O(31)	110.1 (5)
O(26)-K-O(17)	136.4 (1)	C(30)-O(31)-C(32)	111.3 (4)
O(26)-K-O(34)	129.8 (1)	O(31)-C(32)-C(33)	110.7 (5)
O(31)-K-O(17)	109.5 (1)	C(32)-C(33)-O(34)	109.2 (4)
O(31)-K-O(23)	147.3 (1)	C(33)-O(34)-C(35)	112.5 (4)
O(1)-K-N(11)	90.7 (1)	O(34)-C(35)-C(36)	109.1 (5)
O(1)-K-N(20)	90.9 (1)	C(35)-C(36)-N(20)	114.1 (5)
O(1)-K-O(14)	150.8 (1)		
O(1)-K-O(17)	149.0 (1)		
O(1)-K-O(23)	74.1 (1)		
O(1)-K-O(26)	66.6 (1)		
O(1)-K-O(31)	73.2 (1)		
O(1)-K-O(34)	63.2 (1)		

Closest Nonhydrogen Distances (Å) between Cation and Anion

K···O(1)	3.162	O(1)···O(26)	3.282
O(1)···O(34)	3.127	O(1)···C(24)	3.452

Comparison between the Geometries of $[Fe_4(NO)_4(\mu_3\text{-}S)_4]^n$ (n = 0, 1−). The one-electron reduction of the neutral parent to its monoanion gives rise to a small but significant geometrical distortion from cubic T_d symmetry toward tetragonal D_{2d} symmetry. The stereochemical details and consequences of this deformation of the Fe_4S_4 core are as follows.

Iron–Iron Distances. Under the idealized tetragonal D_{2d} configuration of the monoanion, the six Fe–Fe distances divide into two groups of two longer and four shorter distances. The two Fe–Fe distances of 2.703 (1) and 2.704 (1) Å with a mean of 2.704

Å are only 0.016 Å longer than the four shorter Fe–Fe distances of range 2.682 (1)–2.695 (1) Å and mean of 2.688 Å. The fact that the mean of 2.693 Å for the *six* Fe–Fe distances in the monoanion is significantly longer by 0.042 Å than that of 2.651 Å for the *six* Fe–Fe distances in the neutral molecule is in harmony with the added electron in the monoanion populating a molecular orbital that is highly antibonding among all *six* iron atoms (vide infra).

Nonbonding Sulfur···Sulfur Distances. Under tetragonal D_{2d} symmetry the six S···S distances of the monoanion break down into a pattern of four longer and two shorter distances inversely related to the pattern of the Fe–Fe distances. The four longer distances range from 3.511 (2) to 3.520 (2) Å with a mean of 3.517 Å, while the two shorter distances of 3.493 (2) and 3.499 (2) Å average to 3.496 Å. The mean of all six S···S distances of 3.510 Å in the monoanion is comparable to the mean of 3.503 Å in the neutral parent.

Iron–Sulfur Distances. The 12 equivalent Fe–S distances in the neutral molecule vary from 2.208 (1) to 2.224 (1) Å. The mean of 2.217 Å is shorter by 0.014 Å than the mean of 2.231 Å in the monoanion in which the 12 Fe–S distances range from 2.221 (2) to 2.239 (2) Å. Under tetragonal D_{2d} symmetry the twelve Fe–S distances in the monoanion are partitioned into two sets consisting of eight equivalent and four equivalent distances; the means of both sets have an identical value of 2.231 Å.

Iron–Nitrogen and Nitrogen–Oxygen Distances. In the neutral molecule, the four Fe–NO bond lengths possess a narrow range of 1.661 (5)–1.666 (5) Å. The mean of 1.663 Å is slightly longer by 0.004 Å than the mean of 1.659 Å in the monoanion, in which the four Fe–NO bond lengths range from 1.655 (5) to 1.663 (5) Å. The average N–O bond length in the neutral molecule of 1.155 Å (range 1.143 (6)–1.171 (6) Å) is slightly shorter by 0.013 Å than the average N–O bond length in the monoanion of 1.168 Å (range 1.162 (6)–1.178 (6) Å). These bond-length changes are in accordance with the expected occurrence of greater $d\pi(Fe) \rightarrow \pi^*(NO)$ backbonding in the monoanion, as indicated in the solution IR spectra by a 60-cm^{-1} decrease in the nitrosyl stretching frequency on going from the neutral parent (1790 cm^{-1} in CH_2Cl_2) to its monoanion (1730 cm^{-1} in CH_2Cl_2).

Bond Angles. In the Fe_4S_4 core of the neutral molecule, the 12 equivalent Fe–S–Fe and 12 equivalent S–Fe–S bond angles average under cubic T_d symmetry to 73.4 and 104.4°, respectively. In the Fe_4S_4 core of the monoanion, the Fe–S–Fe bond angles separate under D_{2d} symmetry into sets of four equivalent and eight equivalent values of 74.6 and 74.1°, respectively, while the S–Fe–S bond angles likewise break down into two sets of four equivalent and eight equivalent values of 103.2 and 104.1°, respectively. The range of Fe–N–O bond angles of 176.8 (5)–178.9 (6)° in the monoanion is similar to that found in the neutral parent.

Comparative Structural-Bonding Relationships of the Fe_4S_4 Cores in the $[Fe_4(NO)_4(\mu_3\text{-}S)_4]^n$ Series (n = 0, 1–) with Those in the $[Fe_4(NO)_4(\mu_3\text{-}S)_2(\mu_3\text{-}NCMe_3)_2]^n$ Series (n = 0, 1–), in the $[Fe_4(\eta^5\text{-}C_5H_5)_4(\mu_3\text{-}S)_4]^n$ Series (n = 0, 1+, 2+), and in the $[Fe_4(SPh)_4(\mu_3\text{-}S)_4]^n$ Series (n = 2–, 3–). The $[Fe_4(NO)_4(\mu_3\text{-}S)_4]^n$ Series vs. the $[Fe_4(NO)_4(\mu_3\text{-}S)_2(\mu_3\text{-}NCMe_3)_2]^n$ Series. The previously given inverse patterns of Fe–Fe bonding and S···S nonbonding distances in the Fe_4S_4 core of the $[Fe_4(NO)_4(\mu_3\text{-}S)_4]^-$ monoanion conform closely to tetragonal D_{2d} symmetry. This distortion from the idealized cubic T_d architecture of the Fe_4S_4 core in $Fe_4(NO)_4(\mu_3\text{-}S)_4$ is consistent with qualitative electronic considerations based upon a metal-cluster model that in the neutral tetramer assumes a formal d^7 Fe(I) configuration for each iron atom by virtue of its coordination with a NO^+ and three S^{2-} ligands. The resulting 28 available iron core electrons are assigned the ground-state electronic configuration $(e + t_1 + t_2)^{16}(a_1 + e + t_2)^{12}(t_1 + t_2)^0$, with the eight lower energy $\pi^*(NO)$-stabilized $(e + t_1 + t_2)$ tetrairon nonbonding orbitals (i.e., those not involved in *direct* Fe–Fe interactions) and the six $(a_1 + e + t_2)$ tetrairon bonding cluster orbitals being completely filled and the six higher-energy $(t_1 + t_2)$ tetrairon antibonding cluster orbitals being unoccoupied. These symmetry arguments give rise to a total Fe–Fe bond order of 6.0, which is in harmony with the Fe_4S_4 core of the neutral tetramer experimentally possessing cubic T_d symmetry with six electron-pair Fe–Fe bond lengths of 2.651 Å (av). Alternatively, $Fe_4(NO)_4(\mu_3\text{-}S)_4$ may be depicted as a 60-electron metal-cluster system,[39] in which 32 bonding ligand electrons from the four two-electron-donor NO^+ ligands and four six-electron-donor S^{2-} ligands are counted along with the 28 electrons from the four d^7 Fe(I) orbitals. This bonding scheme thereby involves the use of 30 so-called cluster valence MO's,[39] which in this case consist of 16 low-energy *filled* iron–ligand *bonding* combinations[40] (of mainly ligand orbital character) and 14 *filled* iron-based MO's (viz., the eight tetrairon nonbonding $(e + t_1 + t_2)$ and six tetrairon bonding $(a_1 + e + t_2)$ cluster orbitals). The corresponding 16 high-energy, *empty* iron–ligand *antibonding* combinations[40] (of mainly iron-based character) are presumed to be much less stable than the 6 *empty* tetrairon antibonding $(t_1 + t_2)$ cluster orbitals, due to metal–ligand interactions being much stronger than metal–metal interactions. The qualitative application of this latter approach, which takes into account the composite metal–ligand and metal–metal interactions, is essentially equivalent to the qualitative metal cluster model, which considers only the metal-based MO's (vide supra) in providing meaningful predictions with regard to the total metal–metal bond order and symmetry of small metal-cluster systems.[3,15] A qualitative MO diagram (Figure 6) can be utilized to interrelate these bonding descriptions in correlating the electronic configurations for various cubanelike $[M_4(NO)_4(\mu_3\text{-}X)_4]^n$ complexes with their observed geometries.

The reduction of the 60-electron $Fe_4(NO)_4(\mu_3\text{-}S)_4$ to its 61-electron monoanion is then presumed under T_d symmetry to involve the addition of the unpaired electron to the LUMO that corresponds under the metal-cluster model to the tetrairon antibonding triply degenerate t_1 level (i.e., based upon quantitative MO calculations[41] of $Fe_4(NO)_4(\mu_3\text{-}S)_4$ with the Fenske–Hall model,[42] for which the t_1 level was found to lie lower in energy than the t_2 level). The metal-cluster model thereby points to a decrease of the overall metal–metal bond order from 6.0 in the neutral parent to 5.5 in the monoanion, by which a significant increase in the overall average Fe–Fe bond length would be expected. Furthermore, the resulting orbitally degenerate $^2T_1$ ground state in the monoanion can distort the Fe_4S_4 core via a Jahn–Teller active vibration from cubic T_d symmetry to the tetragonal D_{2d} symmetry observed in the monoanion. This symmetry lowering splits the t_1 level into two levels $(a_2 + e)$ with the unpaired electron being placed in the nondegenerate a_2 level. Thus, a preferential elongation of either two or four of the six Fe–Fe distances is predicted in order to conform to D_{2d} symmetry.

An examination of Table V, which compares the mean Fe–Fe and Fe–S bond lengths for the $[Fe_4(NO)_4(\mu_3\text{-}S)_4]^n$ series (n = 0, 1–) and other related series (vide infra), provides experimental evidence in support of the predictions gleaned from the metal-cluster model. The small but significant tetragonal D_{2d} distortion of the Fe_4S_4 architecture in the monoanion is displayed from the experimentally determined pattern of two longer Fe–Fe distances of 2.703 (1) and 2.704 (1) Å vs. four shorter Fe–Fe distances of range 2.682 (1)–2.690 (1) Å. The corresponding means of 2.704 and 2.688 Å are both longer than the mean of 2.651 Å for the six Fe–Fe distances in the neutral tetramer by 0.053 and 0.037 Å, respectively. Hence, the determined Fe–Fe bond-length

(39) Lauher, J. W. *J. Am. Chem. Soc.* **1978**, *100*, 5305–5315.

(40) The 16 metal–ligand bonding and 16 metal–ligand antibonding MO's in $Fe_4(NO)_4(\mu_3\text{-}S)_4$ arise from the interactions of a set of 16 group-donor $(2a_1 + e + t_1 + 3t_2)$ orbitals, formed from the combinations under T_d symmetry of four tetrahedral-like NO^+ and S^{2-} donor orbitals about each Fe(I), with a matching set of higher energy tetrairon symmetry orbitals of 4s and 4p Fe AO character. This description thereby ignores the four unshared electron pairs on the S^{2-} ligands. Since mixing between the orbitals of the same representations can occur to give highly delocalized MO's, these bonding models do not necessarily distinguish the specific nature of the metal–metal bonds, but they do stress the importance of the number and nature of the antibonding metal-cluster electrons in furnishing qualitative assessments of the total metal bonding capacity as well as symmetry of the metal cluster core.

(41) Campana, C. F. Ph.D. Thesis, University of Wisconsin—Madison, Madison, WI, 1975. Campana, C. F.; Block, T. F.; Dahl, L. F., to be submitted for publication.

(42) Hall, M. B.; Fenske, R. F. *Inorg. Chem.* **1972**, *11*, 768–775.

Table V. Comparison of Fe–Fe and Fe–X Distances (Å) for the Idealized Geometries of the Fe_4X_4 Cores in the $[Fe_4(NO)_4(\mu_3\text{-}S)_4]^n$ and $[Fe_4(NO)_4(\mu_3\text{-}S)_2(\mu_3\text{-}N\text{-}t\text{-}Bu)_2]^n$ Series (n = 0, 1–), in the Two $[Fe_4(SR)_4(\mu_3\text{-}S)_4]^n$ Series (R = Ph, CH_2Ph; n = 2–, 3–), in the $[Fe_4(\eta^5\text{-}C_5H_5)_4(\mu_3\text{-}S)_4]^n$ Series (n = 0, 1+, 2+), and in the $[Fe_4(S_2C_2(CF_3)_2)_4(\mu_3\text{-}S)_4]^{2-}$ Dianion

series	Fe–Fe dist[n]	overall Δ(Fe–Fe)	Fe–S dist[n]	overall Δ(Fe–S)	Fe–N dist[n]	overall Δ(Fe–N)
$[Fe_4(NO)_4(\mu_3\text{-}S)_4]^n$						
$n = 0$[a] (T_d Fe_4S_4 core)	[6] 2.651		[12] 2.217			
$n = -1$[b] (D_{2d} Fe_4S_4 core)	[2] 2.704 [4] 2.688	+0.042	[4] 2.231 [8] 2.231	+0.014		
	[6] 2.693[o]		[12] 2.231[o]			
$[Fe_4(NO)_4(\mu_3\text{-}S)_2(\mu_3\text{-}NR)_2]^n$ (where R = CMe_3)						
$n = 0$[c] (C_{2v} $Fe_4S_2N_2$ core)	Fe_2S_2 [1] 2.642		Fe_2S_2 [4] 2.224		Fe_2SN [2] 1.914	
	Fe_2SN [4] 2.562		Fe_2SN [2] 2.222		Fe_2N_2 [4] 1.908	
	Fe_2N_2 [1] 2.496		[6] 2.223[o]		[6] 1.910[o]	
	[6] 2.564[o]					
$n = -1$ (C_{2v} $Fe_4S_2N_2$ core)	Fe_2S_2 [1] 2.701		Fe_2S_2 [4] 2.249		Fe_2SN [2] 1.855	
	Fe_2SN [4] 2.574	+0.028	Fe_2SN [2] 2.260	+0.030	Fe_2N_2 [4] 1.890	−0.032
	Fe_2N_2 [1] 2.552		[6] 2.253[o]		[6] 1.878[o]	
	[6] 2.592[o]					
$Fe_4(SPh)_4(\mu_3\text{-}S)_4]^n$						
$n = -2$[e] (D_{2d} Fe_4S_4 core)	[2] 2.730		[8] 2.296			
	[4] 2.739		[4] 2.267			
	[6] 2.736[o]		[12] 2.286[o]			
$n = -3$,[f] anion 1 (D_{2d} Fe_4S_4 core)	[2] 2.735	+0.007	[8] 2.286	+0.023		
	[4] 2.748		[4] 2.354			
	[6] 2.743[o]	+0.008	[12] 2.309[o]	+0.023		
$n = -3$,[f] anion 2 (D_{2d} Fe_4S_4 core)	[2] 2.726		[8] 2.290			
	[4] 2.753		[4] 2.348			
	[6] 2.744[o]		[12] 2.309[o]			
$[Fe_4(SCH_2Ph)_4(\mu_3\text{-}S)_4]^n$						
$n = -2$[g] (D_{2d} Fe_4S_4 core)	[2] 2.776		[8] 2.310			
	[4] 2.732		[4] 2.239			
	[6] 2.747[o]		[12] 2.286[o]			
$n = -3$[h] (C_{2v} Fe_4S_4 core)	[1] 2.719		[4] 2.317			
	[4] 2.764	+0.012	[4] 2.301	+0.030		
	[1] 2.782		[4] 2.331			
	[6] 2.759[o]		[12] 2.316[o]			

$[Fe_4(\eta^5\text{-}C_5H_5)_4(\mu_3\text{-}S)_4]^n$							
$n = 0$, monoclinic (D_{2d} Fe_4S_4 core)	[2] 2.650					[8] 2.204	
	[4] 3.363					[4] 2.250	
	[6] 3.125[a]					[12] 2.219[a]	
$n = 0$,[j] orthorhombic (D_{2d} Fe_4S_4 core)	[2] 2.631					[8] 2.206	
	[4] 3.366					[4] 2.256	
	[6] 3.121[a]		−0.072			[12] 2.223[a]	−0.005
$n = +1$[k] (D_2 Fe_4S_4 core)	[2] 2.652					[4] 2.185	
	[2] 3.188		−0.068			[4] 2.212	−0.009
	[2] 3.319					[4] 2.246	
	[6] 3.053[a]					[12] 2.214[a]	
$n = +2$[l] (D_{2d} Fe_4S_4 core)	[2] 3.254		−0.079			[8] 2.208	−0.023
	[4] 2.834					[4] 2.156	
	[6] 2.974[a]					[12] 2.191[a]	
$[Fe_4(S_2C_2R_2)_4(\mu_3\text{-}S)_4]^n$ (where R = CF_3)							
$n = -2$[m] (D_{2d} Fe_4S_4 core)	[2] 3.224					[8] 2.247	
	[4] 2.730					[4] 2.153	
	[6] 2.895[a]					[12] 2.216[a]	

[a] This work. [b] $[K(2,2,2\text{-crypt})]^+$ salt; this work. [c] Reference 12. [d] $[(Ph_3P)_2N]^+$ salt; ref 12. [e] $[NMe_4]^+$ salt; ref 46. [f] $[NMeEt_3]^+$ salt; ref 47. [g] $[NEt_4]^+$ salt; ref 13. [h] $[NEt_4]^+$ salt; ref 45. [i] Reference 1a. [j] Reference 1b. [k] Br^- salt; ref 2. [l] $[PF_6]^-$ salt; ref 3. [m] $[AsPh_4]^+$ salt; ref 43. [n] Square brackets denote the number of distances having values listed in the right column. [o] Average.

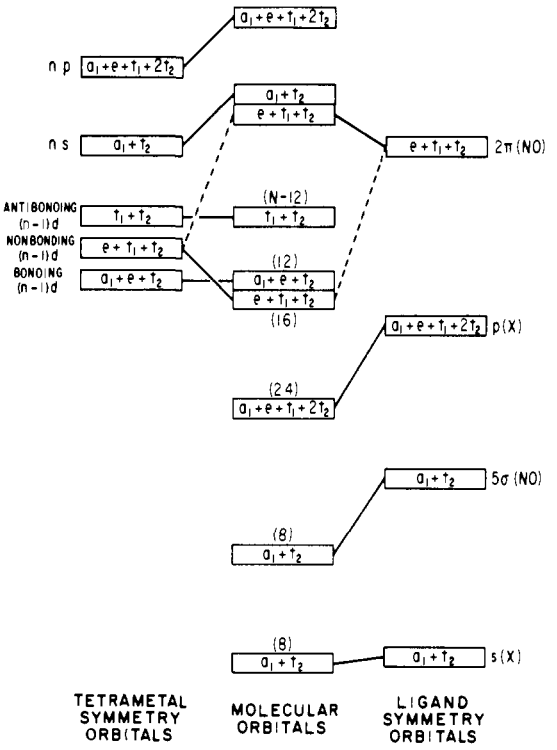

Figure 6. Qualitative MO energy-level diagram (based on MO calculations[41] of $Fe_4(NO)_4(\mu_3\text{-}S)_4$ with the Fenske–Hall model[42]) under cubic T_d symmetry for $[M_4(NO)_4(\mu_3\text{-}X)_4]^n$ complexes containing $12 \le N \le 24$ metal-cluster electrons. For the $[Fe_4(NO)_4(\mu_3\text{-}S)_4]^n$ series ($n = 0, -1$), the neutral parent ($n = 0$) possesses 28 valence iron electrons, of which 16 populate the 2π(NO)-stabilized ($e + t_1 + t_2$) MO's (which are not involved in direct Fe–Fe interactions) while the other 12 populate the ($a_1 + e + t_2$) MO's (which have strongly *bonding* tetrairon orbital character). The latter 12 electrons, which give rise to a completely bonding iron tetrahedron, are thereby denoted as metal cluster electrons. In the reduction to the monoanion (for which $N = 13$), the added electron populates either the t_1 or t_2 MO's (which have strongly *antibonding* tetrairon orbital character). The $N = 13$ electron system is presumed to undergo a Jahn–Teller distortion, for which a first-order vibronic distortion can give rise to the experimentally determined tetragonal D_{2d} Fe_4S_4 configuration. The representation of the tetrametal-bonding $Fe_4(NO)_4(\mu_3\text{-}S)_4$ as a 60-electron system involves the occupation of 30 so-called cluster valence MO's, consisting here of 16 low-energy *filled* iron–ligand bonding combinations ($2a_1 + e + t_1 + 3t_2$) of mainly ligand orbital character and 14 *filled* higher energy iron-based MO's ($a_1 + 2e + t_1 + 2t_2$). This latter description thereby ignores the unshared electron pairs on the four 6-electron donor X^{2-} ligands (where X denotes S), which in the diagram effectively correspond to the four lowest energy MO's ($a_1 + t_2$) resulting primarily from the 4s(X) ligand symmetry orbitals.

elongation in the monoanion does not exclusively involve only two of the six Fe–Fe bonds but instead involves an unequal proportion of both sets of Fe–Fe bonds under D_{2d} symmetry. These changes suggest that the HOMO containing the unpaired electron in the monoanion has considerable tetrairon antibonding character involving all six pairs of iron atoms rather than primarily involving only the two opposite pairs of iron atoms normal to the $S_4\text{-}\bar{4}$ axis. This latter possibility was previously suggested[12] for the $[Fe_4(NO)_4(\mu_3\text{-}S)_4]^-$ monoanion from structural studies[12] of the electronically equivalent $[Fe_4(NO)_4(\mu_3\text{-}S)_2(\mu_3\text{-}NCMe_3)_2]^n$ series ($n = 0, 1-$), for which Table V shows that the C_{2v} cubanelike $Fe_4S_2N_2$ core of the corresponding monoanion exhibits relatively large Fe–Fe bond-length increases of 0.059 Å in the Fe_2S_2 face and 0.056 Å in the Fe_2N_2 face, in contrast to a smaller average Fe–Fe bond-length increase of 0.012 Å in the four equivalent Fe_2SN faces.

In the $[Fe_4(NO)_4(\mu_3\text{-}S)_4]^-$ monoanion, there is a concomitant average increase of only 0.014 Å in the 12 Fe–S bond lengths of the Fe_4S_4 core relative to those in the neutral molecule. Furthermore, the two sets of eight and four equivalent Fe–S bond lengths under D_{2d} symmetry possess identical means of 2.231 Å.

This small overall lengthening in the Fe–S bond lengths relative to the larger Fe–Fe bond-length increases supports the premise that the HOMO of the monoanion has some antibonding iron–sulfur character but that the major driving force producing the redox-generated geometrical perturbations in the Fe_4S_4 core of the $[Fe_4(NO)_4(\mu_3\text{-}S)_4]^n$ series (n = 0, 1−) is primarily a consequence of the variation in metal–metal interactions due to the relatively large tetrairon antibonding orbital character of the HOMO containing the unpaired electron in the monoanion.

The $[Fe_4(NO)_4(\mu_3\text{-}S)_4]^n$ Series vs. the $[Fe_4(\eta^5\text{-}C_5H_5)_4(\mu_3\text{-}S)_4]^n$ Series. Table V reveals that a replacement of the four nitrosyl ligands by four cyclopentadienyl ligands gives rise to four of the six Fe–Fe bond lengths being enlarged by 0.71 Å from electron-pair bonding values of 2.65 Å to nonbonding values of 3.36 Å, with the other two Fe–Fe single-bond lengths remaining constant at 2.65 Å. The resulting alteration in the Fe_4S_4 core from cubic T_d to tetragonal D_{2d} symmetry is in accordance with the metal-cluster model, which has been utilized to correlate the electronic configurations for various cubanelike $[M_4(\eta^5\text{-}C_5H_5)_4(\mu_3\text{-}X)_4]^n$ tetramers[1-9] with their observed geometries. In the case of the neutral $Fe_4(\eta^5\text{-}C_5H_5)_4(\mu_3\text{-}S)_4$ molecule,[1] the 20 3d electrons from the four $3d^5$ Fe(III) orbitals are distributed under T_d symmetry among the 20 3d tetrairon orbitals in the energy-level ordering $(a_1 + e + t_2)^{12}(t_1 + t_2)^8(e + t_1 + t_2)^0$, where the eight tetrametal nonbonding ($e + t_1 + t_2$) combinations have been destablized by the localized octahedral-like ligand field of the tridentate $C_5H_5^-$ and three S^{2-} ligands to higher energies than the six tetrairon antibonding ($t_1 + t_2$) levels.[3] This ground-state electronic configuration containing a *net* total of four tetrametal bonding electrons corresponds to a total Fe–Fe bond order of 2.0, which is in agreement with the observed pattern of Fe–Fe distances. With two tetrairon antibonding electrons partially filling either a triply degenerate t_1 or t_2 level, the observed distortion of the Fe_4S_4 core from the cubic T_d point group to the tetragonal D_{2d} subgroup may be attributed to a first-order Jahn-Teller effect.[3] The description of $Fe_4(\eta\text{-}C_5H_5)_4(\mu_3\text{-}S)_4$ as a 68-electron metal-cluster system is based upon the metal–metal and metal–ligand interactions of the four d^5 Fe(III), the four six-electron-donor S^{2-} ligands, and the four six-electron-donor $C_5H_5^-$ ligands. The 48 ligand-donor electrons populate the 24 low-energy iron–ligand bonding MO's (of principally ligand orbital character), which under T_d symmetry span the representations ($2a_1 + 2e + 2t_1 + 4t_2$), while the 20 metal-based electrons occupy six tetrairon bonding ($a_1 + e + t_2$) and four tetrairon antibonding ($t_1 + t_2$) cluster orbitals. It is apparent from these considerations that the geometrical changes in the Fe_4S_4 core brought about by oxidation of the $Fe_4(\eta^5\text{-}C_5H_5)_4(\mu_3\text{-}S)_4$ parent to either the monocation[2] or dication[3] involve the removal of electrons from the ($t_1 + t_2$) MO's, which are mainly of tetrairon antibonding character. Hence, the major changes encountered in the Fe_4S_4 core of this series should again be reflected primarily in the Fe–Fe distances and secondarily in the Fe–S distances.

The results summarized in Table V are completely consistent with such a description. Each one-electron reduction step of the $[Fe_4(\eta^5\text{-}C_5H_5)_4(\mu_3\text{-}S)_4]^{2+}$ dication to the monocation and then to the neutral tetramer results in a relatively large Fe–Fe bond length increase of 0.07–0.08 Å relative to the Fe–S bond-length increase of 0.01–0.02 Å. The fact that the Fe–Fe bond-length variation in each +2/+1 and +1/0 redox couple of the $[Fe_4(\eta^5\text{-}C_5H_5)_4(\mu_3\text{-}S)_4]^n$ series is nearly twice that in the 0/−1 redox couple of the $[Fe_4(NO)_4(\mu_3\text{-}S)_4]^n$ series may be due to the π-acidic nitrosyl ligands substantially decreasing the tetrairon antibonding character by electron delocalization via the π^*(NO) orbitals. It is also noteworthy that a structural study[43] of the $[Fe_4(S_2C_2(CF_3)_2)_4(\mu_3\text{-}S)_4]^{2-}$ dianion[44] revealed that the pattern of Fe–Fe distances in its Fe_4S_4 core parallels that found[3] in the $[Fe_4(\eta^5\text{-}C_5H_5)_4(\mu_3\text{-}S)_4]^{2+}$ dication, on the basis of which a structural-bonding correlation was given.[43]

The $[Fe_4(NO)_4(\mu_3\text{-}S)_4]^n$ Series vs. the $[Fe_4(SPh)_4(\mu_3\text{-}S)_4]^n$ Series. Both the $[Fe_4(SCH_2Ph)_4(\mu_3\text{-}S)_4]^n$ series (n = 2−,[13] 3−[45]) and the $[Fe_4(SPh)_4(\mu_3\text{-}S)_4]^n$ series (n = 2−,[46] 3−[47]) containing terminal π-donor SR ligands behave entirely differently from the other Fe_4S_4 core-containing series with respect to their redox effect on the Fe_4S_4 geometry in that the −2/−3 electron-transfer couple produces (Table V) relatively large changes in certain Fe–S bond lengths with virtually no changes in the Fe–Fe distances. The two members of these $[Fe_4(SR)_4(\mu_3\text{-}S)_4]^n$ series (R = CH_2Ph,Ph; n = 2−, 3−) have been shown by Holm, Ibers, and co-workers[13,14,45-47] from extensive physicochemical data to be close representations of the prosthetic $Fe_4S_4(SR)_4$ units in certain bacterial ferredoxins (where the terminal SR ligands are cysteinyl groups), which physiologically function as electron carriers via their one-electron redox reactions. Further evidence that the geometries of the dimeric and tetrameric Holm analogues closely model the geometries of corresponding iron–sulfur sites of the proteins in both the solid and solution states was furnished by Teo et al.[48] from EXAFS spectroscopy. The average Fe–Fe and average Fe–S distances of 2.717 (24) and 2.270 (13) Å, respectively, determined from an EXAFS analysis[48] of the $[Fe_4(SCH_2Ph)_4(\mu_3\text{-}S)_4]^{2-}$ dianion (as a microcrystalline powder of the $[NEt_4]^+$ salt), compare favorably not only with the corresponding average values of 2.747 and 2.286 Å obtained from the single-crystal X-ray diffraction analysis[13] but also with those determined from the EXAFS study[48] of the *Clostridium pasteurianum* ferredoxin (solution) in the oxidized form (Fe–Fe, 2.727 (35) Å; Fe–S, 2.249 (16) Å) and in the reduced form (Fe–Fe, 2.744 (32) Å; Fe–S, 2.262 (14) Å).

Whereas the Fe_4S_4 cores of the $[Fe_4(SPh)_4(\mu_3\text{-}S)_4]^{2-}$ and $[Fe_4(SCH_2Ph)_4(\mu_3\text{-}S)_4]^{2-}$ dianions[13,46] are geometrically analogous, those of the corresponding structurally determined trianions[45,47] are not congruent in the crystalline state. The virtually identical Fe_4S_4 cores (Table V) of the two crystallographically independent phenylmercapto trianions in the $[NMeEt_3]^+$ compound were found[47a] to possess an elongated (idealized) tetragonal D_{2d} symmetry. This Fe_4S_4 architecture was shown[47b] from a comprehensive investigation of a number of mercapto analogues by ^{57}Fe Mössbauer, magnetic susceptibility, magnetization, and EPR measurements in the solid state and in frozen acetonitrile solutions to be the intrinsically stable configuration of the $[Fe_4(SR)_4(\mu_3\text{-}S)_4]^{3-}$ trianion in solution. In contrast, the nontetragonal geometry crystallographically observed for the Fe_4S_4 core of the benzylmercapto trianion as the $[NEt_4]^+$ salt was attributed[45,47] to environmental factors in the solid state. Previously established crystal structures[13,46] revealed that the phenylmercapto and benzylmercapto dianions both possess a similar Fe_4S_4 core of compressed (idealized) tetragonal D_{2d} configuration. This inversion of the Fe_4S_4 core from a compressed to an elongated tetragonal D_{2d} geometry upon reduction of the phenylmercapto dianion to the trianion is the consequence of a large 0.084-Å average expansion of the *four* axial Fe–S bonds along the S_4-$\bar{4}$ axis (from 2.267 Å (av) in the independent dianion to 2.351 Å (av) in the two independent trianions) with virtually no concomitant bond-length variations occurring in either the *eight* equatorial Fe–S bonds (≤0.010 Å) or the six Fe–Fe bonds (≤0.008 Å).

The electronic configuration of an $[Fe_4(SR)_4(\mu_3\text{-}S)_4]^{2-}$ dianion may be described as a 54-electron metal cluster system, in which 32 bonding ligand electrons from the four two-electron σ-donor SR^- ligands (i.e., the π-donor mercapto electrons are ignored here) and the four six-electron donor S^{2-} ligands are included together with 22 valence electrons from the experimentally indistinguishable[49] two d^6 Fe(II) and two d^5 Fe(III). Qualitative bonding

(43) Lemmen, T. H.; Kocal, J. A.; Lo, F. Y.-K.; Chen, M. W.; Dahl, L. F. *J. Am. Chem. Soc.* **1981**, *103*, 1932–1941.
(44) Balch, A. L. *J. Am. Chem. Soc.* **1969**, *91*, 6962–6967.
(45) Berg, J. M.; Hodgson, K. O.; Holm, R. H. *J. Am. Chem. Soc.* **1979**, *101*, 4586–4593.
(46) Que, L., Jr.; Bobrik, M. A.; Ibers, J. A.; Holm, R. H. *J. Am. Chem. Soc.* **1974**, *96*, 4168–4178.
(47) (a) Laskowski, E. J.; Frankel, R. B.; Gillum, W. O.; Papaefthymiou, G. C.; Renaud, J.; Ibers, J. A.; Holm, R. H. *J. Am. Chem. Soc.* **1978**, *100*, 5322–5337. (b) Laskowski, E. J.; Reynolds, J. G.; Frankel, R. B.; Foner, S.; Papaefthymiou, G. C.; Holm, R. H. *Ibid.* **1979**, *101*, 6562–6570.
(48) Teo, B.-K.; Shulman, R. G.; Brown, G. S.; Meixner, A. E. *J. Am. Chem. Soc.* **1979**, *101*, 5624–5631.

considerations point to complete occupation of 16 low-energy iron–ligand bonding MO's by the 32 ligand donor electrons with the other 22 electrons filling 11 of the 20 iron-based MO's. Under cubic T_d symmetry a qualitative symmetry-factored MO model[11,13] produces the electronic configuration $(a_1 + e + t_2)^{12}(e + t_1 + t_2)^{10}(t_1 + t_2)^0$ for the 20 iron-based MO's, in which the eight partially filled tetrairon nonbonding $(e + t_1 + t_2)$ orbitals are energetically situated between the filled tetrairon bonding $(a_1 + e + t_2)$ orbitals and the empty tetrairon antibonding $(t_1 + t_2)$ orbitals. This particular electronic configuration thereby gives rise to an Fe_4S_4 core containing a completely bonding tetrahedron of high-spin iron atoms; the 10 electrons in the tetrairon nonbonding $(e + t_1 + t_2)$ orbitals, which are somewhat destabilized by the filled π-donor SR^- orbitals, are assumed by this model to interact with one another via antiferromagnetic spin coupling through the antibonding iron–sulfur orbitals. A qualitative antiferromagnetic spin-coupling model[50] consistent with subsequent Mössbauer studies was later applied by Holm and co-workers[47a] to account not only for the experimental equivalence[49] of the four iron sites in the $[Fe_4(SR)_4(\mu_3\text{-}S)_4]^{2-}$ dianions but also for the experimental nonequivalence[47] of the four iron sites in the $[Fe_4(SR)_4(\mu_3\text{-}S)_4]^{3-}$ trianions (vide infra).

The above ground-state electronic configuration, derived from these simple theoretical considerations,[11,13] formed the basis for an earlier proposal[11] that the one-electron redox actions of an $[Fe_4(SR)_4(\mu_3\text{-}S)_4]^{2-}$ dianion via either oxidation to the monoanion or reduction to the trianion "should not appreciably alter the Fe–Fe distances", but instead "any observed modification of the tetrairon architecture due to an electron transfer would be mainly an effect of the resulting electronic perturbation directed primarily at the Fe–S framework". Its subsequent corroboration by the above-mentioned geometrical changes in the Fe_4S_4 cores for the reduction of the $[Fe_4(SPh)_4(\mu_3\text{-}S)_4]^{2-}$ and $[Fe_4(SCH_2Ph)_4(\mu_3\text{-}S)_4]^{2-}$ dianions to their corresponding trianions clearly illustrates that the dissimilar electronic configurations imposed on a cubanelike Fe_4S_4 core by terminal π-donor mercapto ligands vs. terminal π-acceptor nitrosyl ligands give rise to strikingly different redox-generated changes in the Fe_4S_4 core geometries.

Comparison of Mössbauer Spectral Data for the $[Fe_4(NO)_4(\mu_3\text{-}S)_4]^n$ and Other Related Series and Resulting Bonding Implications. A room-temperature zero-field Mössbauer spectrum of a polycrystalline sample of $[K(2,2,2\text{-crypt})]^+[Fe_4(NO)_4(\mu_3\text{-}S)_4]^-$ consists of one symmetric quadrupole doublet with an isomer shift (δ) at 0.156 mm/s (relative to metallic iron) and a quadrupole splitting (ΔE) of 0.935 mm/s. The average line width of the two peaks is 0.232 mm/s. These values are distinctly different from those at room temperature recently reported by Sedney and Reiff[51] from an extensive zero- and high-field Mössbauer investigation of both $Fe_4(NO)_4(\mu_3\text{-}S)_4$ and $Fe_4(NO)_4(\mu_3\text{-}S)_2(\mu_3\text{-}NCMe_3)_2$. They hoped to differentiate between the two crystallographically determined types of local iron sites in the latter $Fe_4S_2N_2$ cluster by the expectation of four-line Mössbauer spectra as opposed to the anticipated two-line spectra for $Fe_4(NO)_4(\mu_3\text{-}S)_4$. However, both $Fe_4(NO)_4(\mu_3\text{-}S)_4$ and $Fe_4(NO)_4(\mu_3\text{-}S)_2(\mu_3\text{-}NCMe_3)_2$ gave markedly similar zero-field spectra (over the temperature ranges 4.2–300 K and 1.6–300 K, respectively), consisting of a single symmetric quadrupole-split doublet with δ values (relative to metallic iron) varying from 0.150 (0.141) mm/s (at 78 K) to 0.092 (0.093) mm/s (at 300 K) for the Fe_4S_4 (and $Fe_4S_2N_2$) clusters and with ΔE values of range 1.45–1.47 mm/s for the Fe_4S_4 cluster. These results and the analogous field dependence of the spectra led to the conclusion[51] that both compounds possess very similar environments (with $NCMe_3$ and S ligands thereby producing comparable ligand fields at an iron nucleus), which are equivalent on a Mössbauer time scale. Although the high-field spectra of both compounds gave rise to an internal hyperfine field of zero in accordance with a diamagnetic ground state, temperature-dependent magnetic susceptibility measurements[51] showed a small degree of paramagnetic character with the magnetic moment per iron decreasing from 0.76 to 0.52 μ_B for the Fe_4S_4 cluster and from 0.80 to 0.62 μ_B for the $Fe_4S_2(NR)_2$ cluster over a temperature range of 300–50 K for both compounds.

The above Mössbauer spectral data are completely compatible with crystallographic parameters which show that the neutral $Fe_4(NO)_4(\mu_3\text{-}S)_4$ molecule ideally has cubic T_d symmetry and the $[Fe_4(NO)_4(\mu_3\text{-}S)_4]^-$ monoanion tetragonal D_{2d} symmetry (i.e., the four iron atoms in each of the respective Fe_4S_4 cores are structurally equivalent). Due to the isomer-shift values of the neutral parent being temperature dependent, no bonding correlations within this series are made.

Especially noteworthy is that in the $[Fe_4(\eta^5\text{-}C_5H_5)_4(\mu_3\text{-}S)_4]^n$ series ($n = 0, +, 2+$) the determined isomer shifts[52] remain essentially constant upon change in oxidation state n in contrast to significant variations[47a] in δ upon reductions of the $[Fe_4(SPh)_4(\mu_3\text{-}S)_4]^{2-}$ and $[Fe_4(SCH_2Ph)_4(\mu_3\text{-}S)_4]^{2-}$ dianions to their respective trianions. Whereas Mössbauer spectra[49,53] of various salts of the two $[Fe_4(SR)_4(\mu_3\text{-}S)_4]^{2-}$ dianions display one symmetric quadrupole doublet down to temperatures as low as 1.5 K, Mössbauer spectra[47] of salts of the two corresponding trianions are distinctly different but share a common feature in being characterized as two overlapping (or broadened) quadrupole doublets with different isomer shifts and with temperature-variable quadrupole splittings. Moreover, for comparative zero-field and magnetically perturbed Mössbauer spectral characteristics, Holm, Frankel, and coworkers[47] established a clear similarity between the $[Fe_4S_4(\mu_3\text{-}SPh)_4]^{3-}$ trianion (as the intrinsically stable structural form) and the reduced ferredoxin Fe_4S_4 sites (Fd_{red}) as well as between both structurally congruent dianions and the oxidized ferredoxin Fe_4S_4 sites (Fd_{ox}). Of particular interest is the observed correlation between the isomer shifts of the iron–sulfur sites in the mononuclear, dinuclear, and tetranuclear high-spin iron analogues and proteins and the mean formal oxidation states, in which a monotonic displacement of δ values to increasing positive velocities occurs with decreasing oxidation state. Thus, the $[Fe_4(SPh)_4(\mu_3\text{-}S)_4]^{2-}$ dianion with an average oxidation state of +2.5 (based on 2Fe(II) and 2Fe(III)) has a smaller δ value (0.35 mm/s) (at 77 K relative to metallic iron at room temperature) than the corresponding δ values (0.56 and 0.61 mm/s) for the $[Fe_4(SPh)_4(\mu_3\text{-}S)_4]^{3-}$ trianion, which possesses an average oxidation state of +2.25 (based on 3Fe(II) and 1Fe(III)).[47a] It was proposed[47a] that the equivalence of the four iron sites in the Fe_4S_4 cores of the dianions and Fd_{ox} is consistent with an antiferromagnetic model[50] originally formulated to account for protein ground-state properties. This qualitative description involves the iron atoms being antiferromagnetically coupled in pairs with fast electron hopping ($\tau^{-1} \geq 10^7\ s^{-1}$) between pairs in contradistinction to the two Mössbauer-distinguishable sites in the $[Fe_4(SPh)_4(\mu_3\text{-}S)_4]^{3-}$ trianion and in Fd_{red} arising from the added electron being localized on one pair (2Fe(II)), persistence of rapid hopping within the other pair, and slow electron transfer ($\tau^{-1} \leq 10^7\ s^{-1}$) between pairs.

In the $[Fe_4(\eta^5\text{-}C_5H_5)_4(\mu_3\text{-}S)_4]^n$ series ($n = 0, 1+, 2+$) the observed insensitivity of the Mössbauer parameters to oxidation change (viz., δ values relative to iron metal of 0.30–0.35, 0.35, and 0.35 mm/s, respectively, for $n = 0, 1+, 2+$) may be associated with the redox couples involving MO's that are primarily of tetrairon antibonding character. It is then presumed that the terminal cyclopentadienyl ligands exert a balancing effect on the distribution of electron density in the 4s and 3d Fe AO's such that electron removal upon oxidation of the $Fe_4(\eta^5\text{-}C_5H_5)_4(\mu_3\text{-}S)_4$ molecule to either its monocation or its dication is compensated by increased electron donation, mainly from the cyclopentadienyl ligands, such that no significant *net* changes in electron population

(49) Holm, R. H.; Averill, B. A.; Herskovitz, T.; Frankel, R. B.; Gray, H. B.; Siiman, O.; Grunthaner, F. J. *J. Am. Chem. Soc.* **1974**, *96*, 2644–2646.
(50) Dickson, D. P. E.; Johnson, C. E.; Thompson, C. L.; Cammack, R.; Evans, M. C. W.; Hall, D. O.; Rao, K. K.; Weser, U. *J. Phys. (Paris)* **1974**, *35*, C6-343.
(51) Sedney, D.; Reiff, W. M. *Inorg. Chim. Acta* **1979**, *34*, 231–236.
(52) Wong, H.; Sedney, D.; Reiff, W. M.; Frankel, R. B., Meyer, T. J.; Salmon, D. *Inorg. Chem.* **1978**, *17*, 194–197.
(53) Frankel, R. B.; Averill, B. A.; Holm, R. H. *J. Phys. (Paris)* **1974**, *35*, C6-107.

occur in either the 4s or 3d Fe AO's.

Acknowledgment. This research was made possible by financial support from the National Science Foundation. We are also indebted to Dr. Clifford Feldmann (Department of Chemistry, University of Wisconsin—Madison) for the magnetic susceptibility measurements and to Jonathan Phillips and Professor James A. Dumesic (Department of Chemical Engineering, University of Wisconsin—Madison) for the ^{57}Fe Mössbauer measurements.

Registry No. $Fe_4(NO)_4(\mu_3\text{-}S)_4$, 53276-80-5; $[K(2,2,2\text{-crypt})]^+[Fe_4(NO)_4(\mu_3\text{-}S)_4]^-$, 81583-84-8; $[Co(\eta^5\text{-}C_5H_5)_2]^+[Fe_4(NO)_4(\mu_3\text{-}S)_4]^-$, 81583-82-6; $[AsPh_4]^+[Fe_4(NO)_4(\mu_3\text{-}S)_4]^-$, 81583-83-7; $Hg[Fe(CO)_3NO]_2$, 28411-05-4.

Engineering of Chiral Crystals for Asymmetric ($2_\pi + 2_\pi$) Photopolymerization. Execution of an "Absolute" Asymmetric Synthesis with Quantitative Enantiomeric Yield[1]

Lia Addadi,* Jan van Mil, and Meir Lahav*

Contribution from the Department of Structural Chemistry, The Weizmann Institute of Science, Rehovot, 76100, Israel. *Received August 12, 1981*

Abstract: An "absolute asymmetric synthesis" with quantitative enantiomeric yield, via the process of crystallization of a nonchiral compound in a chiral crystal followed by a topochemical photoreaction, has been successfully executed. The needed crystalline chiral phases, composed of unsymmetrically disubstituted dienes and with the two different double bonds correctly juxtaposed for asymmetric ($2_\pi + 2_\pi$) photodimerization and photopolymerization along a translational axis, were designed. The starting point for this matrix engineering was the crystal structure of the chiral monomer **1**. After inspection of the shortest contacts made by the chiral *sec*-butyl group inside the crystal, we examined some hypothetical transfers of methyls to and from this group, with the nearest neighboring molecules; such transfers might generate phases isomorphous to **1** but composed of achiral monomers. Four systems were considered promising candidates, namely the 1:1 mixture of monomers **3** and **4** and monomers **8**, **9**, and **11**. Three of these behave in the predicted way. Large single crystals of achiral monomer **9** were grown and irradiated, yielding, in a number of independent experiments, dimers and oligomers of either chirality, with a quantitative enantiomeric yield within the limits of experimental error.

Introduction and Statement of the Problem

This work is part of a program on the design and execution of an "absolute asymmetric synthesis", i.e., an asymmetric synthesis carried out in a closed system in the absence of any external chiral inducing agents.[1-4] The strategy of the present approach is outlined in Scheme I.

We shall consider a nonchiral monomer that crystallizes into an enantiomorphous crystal, where the photopolymerizable molecules are correctly aligned and juxtaposed so as to undergo topochemical reactions with the formation of products of a single chirality. In such a case, the asymmetric induction would be due to the chirality of the crystalline matrix only.

The model structural motif proposed is based on 1,4-disubstituted phenylenediacrylates with two different substituents, X and Y, packed in a chiral crystal in such a way that translationally related neighboring molecules have nonequivalent double bonds parallel and at the correct distance (4 Å) needed for photocyclodimerization and polymerization. The problem of engineering the desired motif was simplified by splitting it into a number of steps. First, we built the crystalline matrix needed for the reaction using chiral resolved monomer **1** (cell constants are listed in Table I) and studied its behavior as a model system. The use of a resolved monomer in this first stage guaranteed packing in a chiral crystal and greatly simplified the search for a valid motif. In a previous communication we showed that **1** meets all the predetermined requirements and yields upon irradiation chiral dimers **2** (Scheme II), trimers, and oligomers with the expected stereochemistry and with quantitative diastereomeric yield.[2] We proposed in a second step to modify this monomer molecule in such a way as to generate one or more monomers of the same family, packing in structures isomorphous to **1** but containing nonchiral or racemic handles. This was, until now, only partially accomplished.[1a] We describe here a path to the successful accomplishment of the second step, which leads to the first absolute asymmetric synthesis with quantitative enantiomeric yield.

Results and Discussion

In the present approach we exploit the information contained in the crystal structure of **(*S*)-(+)-1**[5] (Figures 1, 4, and 5). The purpose is to determine, on paper, which molecular changes performed on **1** would eliminate the chiral center of the *sec*-butyl handle, while maintaining almost the same overall occupied-molecular volume and the same interactions within the lattice (the principle of isomorphous replacement). We consider, therefore, all of the short contacts (< 5 Å) in which the chiral *sec*-butyl is

(1) Photopolymerization in Chiral Crystals 4. For part 3, see: (a) L. Addadi and M. Lahav, *J. Am. Chem. Soc.*, **101**, 2152 (1979). This work has been presented, in part, in the form of plenary lectures at the Second IUPAC Conference on Organic Synthesis, Jerusalem, 1978[1b] and at the 62nd Meeting of the Canadian Chemical Society, Vancouver, 1979.[1c] (b) L. Addadi and M. Lahav, *Pure App. Chem.*, **51**, 1269 (1979). (c) L. Addadi and M. Lahav, *Stud. Phys. Theor. Chem.*, **7**, 179 (1979).

(2) L. Addadi and M. Lahav, *J. Am. Chem. Soc.*, **100**, 2838 (1978).

(3) L. Addadi, E. Gati, M. Lahav, and L. Leiserowitz, *Isr. J. Chem.*, **15**, 116 (1976/77).

(4) For other examples of absolute asymmetric synthesis by solid state topochemical reactions, see (a) A. Elgavi, B. S. Green, and G. M. J. Schmidt, *J. Am. Chem. Soc.*, **95**, 2058 (1973); (b) K. Penzien and G. M. J. Schmidt, *Angew. Chem., Int. Ed. Engl.*, **8**, 608 (1969).

(5) Z. Berkovitch-Yellin, *Acta Crystallogr., Sect. B*, **B36**, 2440 (1980).

0002-7863/82/1504-3422$01.25/0 © 1982 American Chemical Society